Noise reduction and spatial resolution in CT imaging with the ASIR iterative reconstruction algorithm at different doses and contrasts - a phantom study.

Poster No.:	C-0862
Congress:	ECR 2016
Type:	Scientific Exhibit
Authors:	M. E. Fantacci, P. Barca, M. Giannelli, D. Giustini, C. Sottocornola, D. Caramella; Pisa/IT
Keywords:	Quality assurance, Physics, CT, Radioprotection / Radiation dose
DOI:	10.1594/ecr2016/C-0862

Aims and objectives

In the last few years, Computed Tomography (CT) has became an essential diagnostical imaging technique, which daily helps to save many lives. However, in industrialized countries, CT is the largest source of population exposure to ionizing radiation. For this reason, part of the interest of scientific community is focused on the optimization of CT radiation dose. In this context, modern CT scanners adopt many scanning-related techniques of dose reduction, like automatic tube current modulation. In addition, another approach for dose reduction is represented by the improvement of image reconstruction algorithms. In fact, recent advances in CT imaging include the development of iterative reconstruction algorithms in order to obtain a dose reduction without compromising the diagnostic quality of images compared to conventional filtered back projection (FBP) reconstructed images [9]. In contrast with FBP algorithm, IR algorithms take into account a model of the imaging system to describe the different physical aspects of image acquisitions. This leads to a better description of the imaging process and thus may offer the opportunity to reduce image noise with respect to FBP reconstructions. Because of the strict relationship between image noise and radiation dose, IR algorithms could provide a dose reduction without affecting the spatial resolution performance.

Many IR algorithms are already in use in CT clinical applications, so there is the need to investigate the actual dose reduction potential and imaging proprieties of these new recontruction tecniques.

In this work, we focus our attention on the ASIR (Adaptive Statistical Iterative Reconstruction, GE Healthcare) algorithm, which is widely used in clinical practice. ASIR is an IR algorithm that works on raw data space modeling the fluctuations in the projection measurement, due to limited photon statistics, and the noise characteristics of the scanned object (e.g. scattring) [9, 10]. ASIR offers the possibility of blending with FBP at various levels, from 0% (conventional FBP) to 100% ("pure" ASIR).

Previous works have shown various peculiar image quality properties of ASIR-reconstructed images with respect to FBP-reconstructed images [3-5, 12]. In fact, the noise reduction in the ASIR-reconstructed images is accompanied by changes in the noise texture, leading to a different image appearence, and the spatial resolution can vary as a function of dose and contrast. In these works, only one or a few percentages of ASIR were considered.

In our work, we performed a quantitative noise analysis using different ASIR percentages and a wide range of the main scanning parameters (i.e. tube load, kilovoltage, pitch, slice thickness) values. The Noise Power Spectra (NPS) were computed to take into account any changes in noise texture. Spatial resolution was assessed by computing the Modulation Transfer Function (MTF) from images reconstructed with different percentages of ASIR, for a wide range of scanning parameters values and different contrasts.

The purpose of our work was to assess noise reduction and spatial resolution in CT ASIR-reconstructed images, in order to evaluate the real dose reduction potential of this new algorithm in different scanning situations.

Methods and materials

In this work, we used a 64-slice CT scanner (PET/CT Discovery 710, GE Healthcare) to acquire images of a Catphan-504 phantom (The Phantom Laboratory). This phantom has a cylindrical shape with an internal diameter of 15 cm and it is composed of 4 modules, as shown in Fig. 1 on page 12.

For our tasks we used three modules of the phantom: the CTP486 module is a homogeneous water-equivalent modolus, whose axial images are shown in Fig. 2 on page 12; the CTP404 module contains many inserts of various material in a water-equivalent background (nominal CT HU of these inserts are shown in Tab. (1), two pair of 23° wire ramps, many acrylic spheres and air and Teflon rods Fig. 3 on page 13; the CTP528 module has a 1 through 21 line pair per centimeter and two tungsten carbide beads with a diameter of 0.28 mm, which are cast into a uniform material Fig. 4 on page 14.

Material	**HU range (reference values)**
Air	-1046 : -986
PMP	-220 : -172
LDPE	-121 : -87
Polystyrene	-65 : -29
Acrylic	92 : 137
Delrin	344 : 387
Teflon	941 : 1060
Background (measured value)	95 +/- 7

Table 1: HU values of the CTP404 module inserts.

For noise analysis, the CTP486 module of the phantom was scanned using a reference protocol and varying the main scanning parameters on a wide range of values (Tab. 2). For spatial resolution analysis both CTP404 and CTP528 modules were used. The CTP404 module was scanned across a wide range of tube current values (40, 80, 120, 160, 200, 240, 280 and 320 mA) and using the scanning protocol values shown in Tab. 3, while the CTP528 modolus was scanned using another protocol, shown in Tab. 4.

Images were reconstructed both by conventional FBP (with the GE "standard" filter) and ASIR at various percentages (20%, 40%, 60%, 80%, 100%) of blendig. Note that, in our case, the ASIR reconstruction was a "retro-reconstruction" made from the same raw data used for FBP.

Image analyses were performed with ImageJ (US National Institute of Health) software and Origin (OriginLab) software.

Scan protocol for the noise analysis

Acquisition mode:	spiral
Tube current (mA):	100
Kilo-voltage (kV):	120
Tube rotation time (s):	0.7
Slice thickness (mm):	2.5
Collimation along longitudinal direction (mm):	40
Pitch:	0.984
Scan Field Of View:	Large Body
Display Field Of View (mm):	420
Filtration:	GE standard filter

(a)

Variations of scanning parameter values

Tube current (mA):	40, 60, 80, 120, 140, 160
Kilo-voltage (kV):	80, 100, 140
Slice thickness (mm):	0.625, 1.25, 3.75, 5, 7.5

Pitch:	0.516, 1.375

(b)

Table 2: Reference protocol (a) and variations of scanning parameter values (b) used for the noise analysis.

Acquisition mode:	spiral
Tube current (mA):	40, 80, 120, 160, 200, 240, 280, 320
Kilo-voltage (kV):	120
Tube rotation time (s):	0.7
Slice thickness (mm):	2.5
Collimation along longitudinal direction (mm):	40
Pitch:	0.984
Scan Field Of View:	Head (320 mm)
Display Field Of View (mm):	210
Filtration:	GE standard filter

Table 3: Scan protocols for the spatial resolution analysis using the CTP404 module of the Catphan 504 phantom.

Acquisition mode:	spiral
Tube current (mA):	320
Kilo-voltage (kV):	120
Tube rotation time (s):	0.7
Slice thickness (mm):	2.5
Collimation along longitudinal direction (mm):	40
Pitch:	0.984
Scan Field Of View:	Head (320 mm)

Display Field Of View (mm):	50
Filtration:	GE standard filter

Table 4: Scan protocols for the spatial resolution analysis using the CTP528 module of the Catphan 504 phantom.

1) Noise analysis

It is well know that in CT imaging there are many noise sources which can affect the image quality. However, the main source of noise is represented by quantum or statistical noise, which arises from the detection of a finite and random number of x-ray photons (N) in the data acquisition process. The N number is influenced by different scanning parameters such as tube current, exposure time, kilovoltage, pitch and slice thickness, and depends on the detector efficiency and x-ray tube performance. In most situations the distribution of the number of detected x-ray quanta is well approximated by a Poisson distribution [1, 2], thus it is expected that the noise in the images is proportional to 1/ sqrt(N) and thus it's also expected that the noise is related to the radiation dose by an inverse square root low.

Theoretically, the image noise should be measured computing the standard deviation from an ensamble of images, acquired at the same scanning conditions. Nevertheless, the simplest and fastest way to measure the image noise in CT is to compute the standard deviation over a ROI of the image. However, this method doesn't take into account the correlation of noise in the images that is at the origin of noise texture appearence. For this reason, for a complete noise analysis, it is necessary to calculate the auto-correlation function or, equivalently, its Fourier transform (FT), i.e. the noise power spectrum (NPS).

The NPS for digital images can be defined as [6]

$$NPS\left(f_x,f_y,f_z\right)=\frac{\Delta x\Delta y\Delta z}{N_x N_y N_z}\left\langle\left(\left|FFT\left(VOI\left(x,y,z\right)\right)\right|\right)^2\right\rangle$$

(1)

in which #x, #y and #z are the dimensions of the voxels in x, y and z directions; f_x, f_y, f_z are spatial frequencies; N_x, N_y, N_z are the number of pixels in each direction; FFT stands

for a 3D Fast Fourier Transform and <*> indicates an ensamble average. The VOI(x,y,z) which appears in equation (1) represents a "only-noise" VOI.

The eq. (1) defines a three-dimensional (3D) NPS, which is most appropriate for modern CT imaging tecnique because of its intrinsic 3D nature. However, is almost always preferred a 2D approach, because it offers a clearer interpretation of the noise spatial correlation proprieties. The 2D NPS is defined as [7]

$$NPS\left(f_x,f_y\right)=\frac{\Delta x\Delta y}{N_x N_y}\left\langle\left(\left|FFT\left(ROI\left(x,y\right)\right)\right|\right)^2\right\rangle$$

(2)

In this work, noise performance of ASIR were evaluated by measuring the standard deviation (SD) on a region of interest (ROI) in the recontructed images and computing the 3D, 2D and 1D NPS.

The SD calculations were performed on a circular ROI (4.5 cm diameter corresponding to 30% of the internal phantom diameter) centered in the images as shown in fig. (5). Starting from the reference protocol (Tab. 2a), we varied the main scanning parameter values (Tab. 2b) in data acquisitions and we compared the SDs of FBP-reconstructed images with SDs of ASIR-rconstructed images.

We also performed an NPS calculation from images acquired with the reference protocol (Tab. 2a), using eq. (1) and eq. (2) . The "only-noise" images were computed subtracting one set of images from another set of images acquired with the same scanning parameter values.

For the 3D NPS calculation we used an ensamble of 20 volumes of interest (VOI) selected from 19 consecutive slices. The physical dimensions of each VOI were 52.5x52.5x17.5 mm^3. In fact, in the axial plane each VOI had a 64x64 pixels surface (52.5x52.5 mm^2), and was partially overlapped (up to 50%) with each other as shown in Fig. 6 on page 15; along the longitudinal direction, the VOI were composed of 7 pixels and each one overlapped the previous and next VOI by 3 pixels (except for the first and last VOI). Note that the pixels dimensions in the axial plane were 0.82 mm (equal to the ratio between the display field of view dimension and the matrix size), while along the longitudinal direction the pixels dimension is equal to the slice thickness (2.5 mm in this case). From each VOI we calculated the 3D NPS and then we made an ensamble average.

To compute the 2D NPS was considered only the central slice of 19, and we chose 5 partially overlapped ROI (up to 50%), as shown in Fig. 6 on page 15. The physical dimensions of each ROI was 52.5x52.5 mm^2 (corrisponding to 64x64 pixels). The 2D NPS was calculated (using eq. 2) from each ROI and then we made an average over the 5-ROI ensemble.

Once 2D NPS has been calculated (or a 2D frequency plane of 3D NPS selected), we performed a radial average and obtained a 1D NPS curve.

To evaluate any changes in NPS shape and magnitude related to ASIR reconstruction, we compared the noise power spectra from ASIR-reconstructed images (at various percentages of reconstruction) to FBP-reconstructed images.

2) Spatial resolution analysis

All imaging systems introduce blurring in the images, which is the expression of physical phenomena that occur during the imaging process. In CT systems, the spatial resolution is limited by many factors related to data acquisition and images reconstruction.

The spatial resolution in CT imaging can be evaluated in the spatial domain measuring the point spread function (PSF) of the system. However, in most situations it is useful to assess the spatial resolution in the spatial frequency domain through the calculation of the modulation transfer function (MTF). The MTF is simply related to the "line per mm" concept of resolution and it is also often difficult to measure the PSF. For these reasons, the MTF metric is widely used in CT imaging to evaluate spatial resolution. The MTF describes how the imaging system transfers the contrast across spatial frequencies and it is simply related to the PSF:

$$MTF\left(f_x, f_y\right) = \left| FT\left(PSF\left(x,y\right)\right)\right|$$

(3)

Equivalently, the MTF can be defined as the ratio of output and input modulations:

$$M = \frac{I_{max} - I_{min}}{I_{max} + I_{min}}$$

(4)

where "I" stands for instensity of the grey levels in the images.

As we said previously, it is not always simple to measure the PFS. For this reason, often, the MTF is computed through measures of the line spread function (LSF) or of the edge spread function (ESF). These functions are related with the PSF, in fact:

$$LSF(x) = \int PSF(x,y)\,dy$$

(5)

$$ESF(x) = \int_{-\infty}^{x} LSF(x')\,dx'$$

Thus, the MTF can be calculated by [3]:

$$MTF(f) = \left(\frac{\int [d(ESF(x))/dx] \exp(-2\pi i f x)\, dx}{\int [d(ESF(x))/dx]\, dx} \right)$$

(6)

in which "f" represents the spatial frequency along a given direction.

The use of the MTF as a metric to assess spatial resolution is formally restricted to linear and shift invariant systems. CT systems, in general, are not shift invariant systems, because the resolution can vary over the image plane [2]. Moreover, while the FBP is a linear recontruction algorithm, IR algorithms are intrinsically nonlinear (e.g. they take into account nonlinear phenomena shuch as scattering). Also note that a "standard" FBP reconstruction could be nonlinear due to the beam hardening correction [11]. Therefore an intrinsic assunption is done when an MTF-based method is used to assess spatial resolution in CT system (i.e. the system is considered linear and shift invariant).

Previous works have shown that the MTF is dose- and contrast-dependent when using ASIR algorithm but not FBP algorithm and this behaviour was attributed to the nonlinear signal characteristics of the IR algoritms [3-5, 12].

To carefully investigate these aspects of ASIR algorithm, we performed an MTF analysis at various dose and contrast levels. We used two methods for MTF calculations.

In the first method, images of CTP404 module (see Fig. 3 on page 13) were acquired with the scanning parameters in tab. 3 and reconstructed both with FBP and different percentages of ASIR (20%, 40%, 60%, 80%, 100%). The CTP404 module has 8 circular inserts with diameters of approximately 13.5 mm; we used six of these inserts (i.e. Air, PMP, LDPE, Polystyrene, Delrin and Teflon) to perform MTF calculations through the circular edge method:

1. a circular ROI with a diameter twice that of the inserts was centered on each insert (see Fig. 7 on page 16) and a radial profile average was computed to obtain the ESF;
2. the ESF was fitted using a sigmoidal function:

$$f(x) = \frac{A - B}{1 + \exp\left((x - x')/d\right)} + B$$

(an example is shown in Fig. 8 on page 17);

3. a discrete derivative of the fitting function was computed to obtain the LSF;
4. the MTF was computed as the module of the fast Fourier transform (FFT) of the LSF;
5. steps 1. to 4. were repeated for 7 "identical" images acquired with the same scanning parameters and the MTF curves corrisponding to the same insert were averaged and normalized to the MTF value at zero frequency.

The second method was the standard PSF method which we used as a "verification" of the circular edge method. The module CTP528 contains a 0.28 diameter bead serving as a point source for PSF measures. The CTP528 section was scanned using the parameters in Tab. 4. In this case we set a small Display Field of View (5 cm) to better detect the bead location, while the Scan Field of View was the same of the CTP404 scan. The MTF was computed as follow:

1. a square ROI (64x64 pixels, corrisponig to physical dimensions of 6.25x6.25 mm^2) was centerd on the PSF and 64 horizontal profiles were averaged to obtain the LSF (see Fig. 9 on page 18);
2. the LSF was fitted using a gaussian function:

$$f(x) = y_0 + \frac{A}{w\sqrt{\frac{\pi}{2}}} \exp\left(-2\left(\frac{x - x_c}{w}\right)^2\right)$$

(an example is shown in Fig. 10 on page 19);

3. the background was subtracted from the LSF;
4. the MTF was computed as the module of the FFT of the LSF;

5. steps 1. to 4. were repeated for 7 "identical" images acquired with the same scanning parameters and the MTF curves were averaged and normalized to the MTF value at zero frequency.

The images of CTP528, acquired for the "verification" method, were reconstructed with FBP algorithm.

The uncertainties attributed to the MTF were computed as the standard deviation of seven MTF ensamble made from 7 "identical" acquisition.

Note that fitting was necessary to reduce the fluctuations in the tails of the ESF (1st method) and LSF (2nd method) that were more pronounced for low dose acquisitions.

Images for this section:

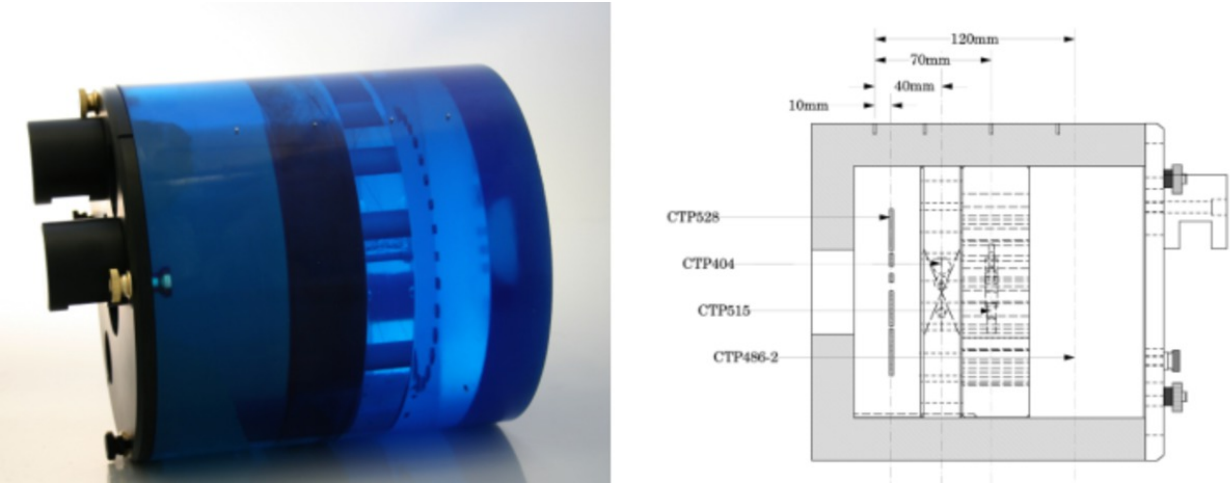

Fig. 1: Representation of the Catphan 504 phantom.

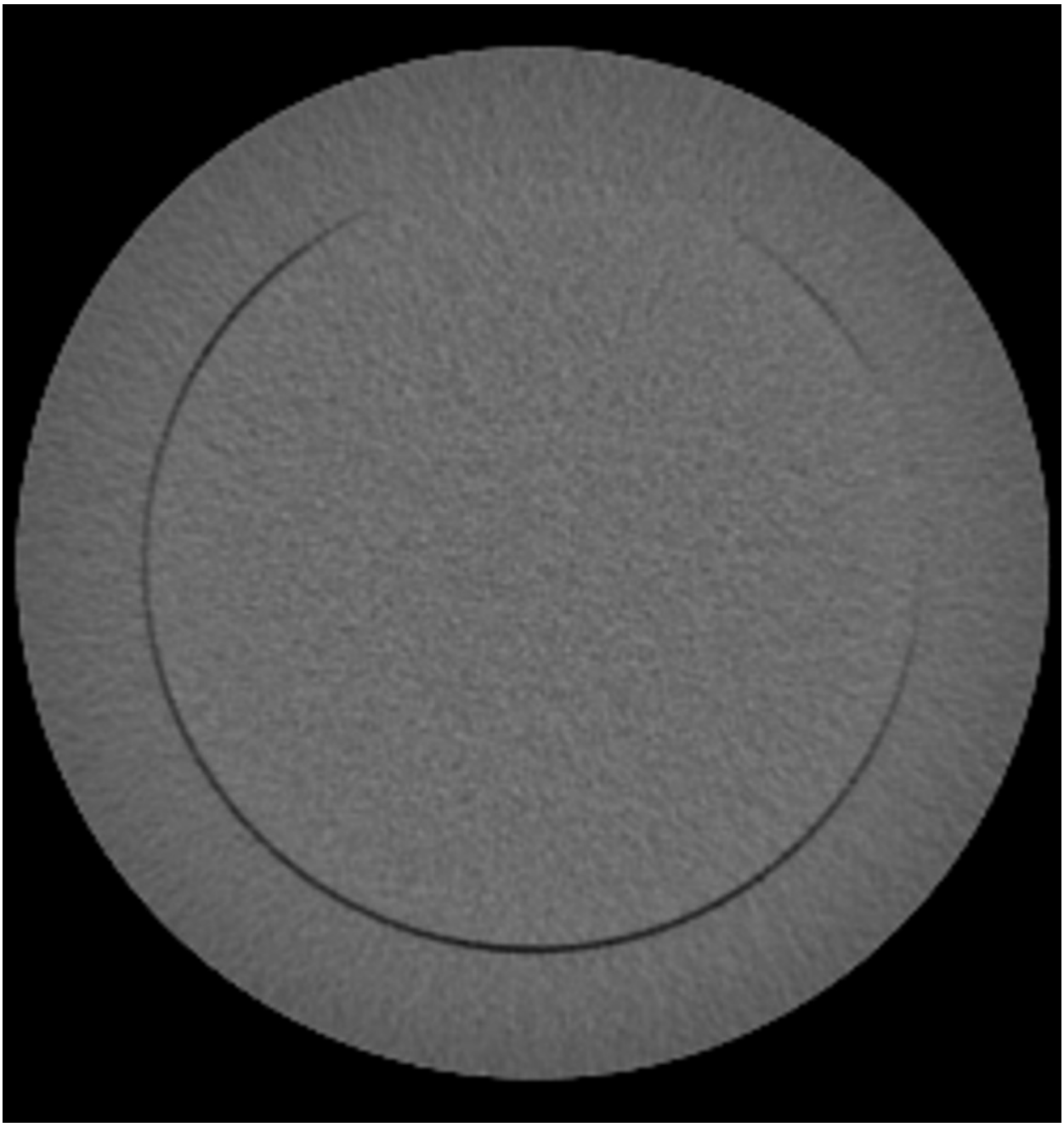

Fig. 2: Image of the CTP486 module of the Catphan 504 phantom.

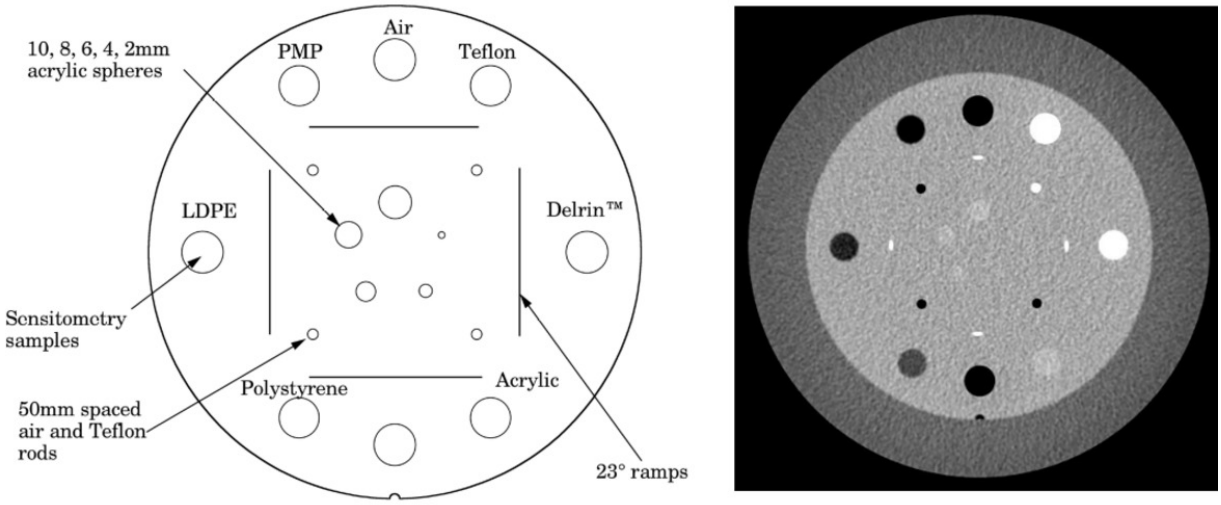

Fig. 3: Module CTP404 of the Catphan 504 phantom.

© - Pisa/IT

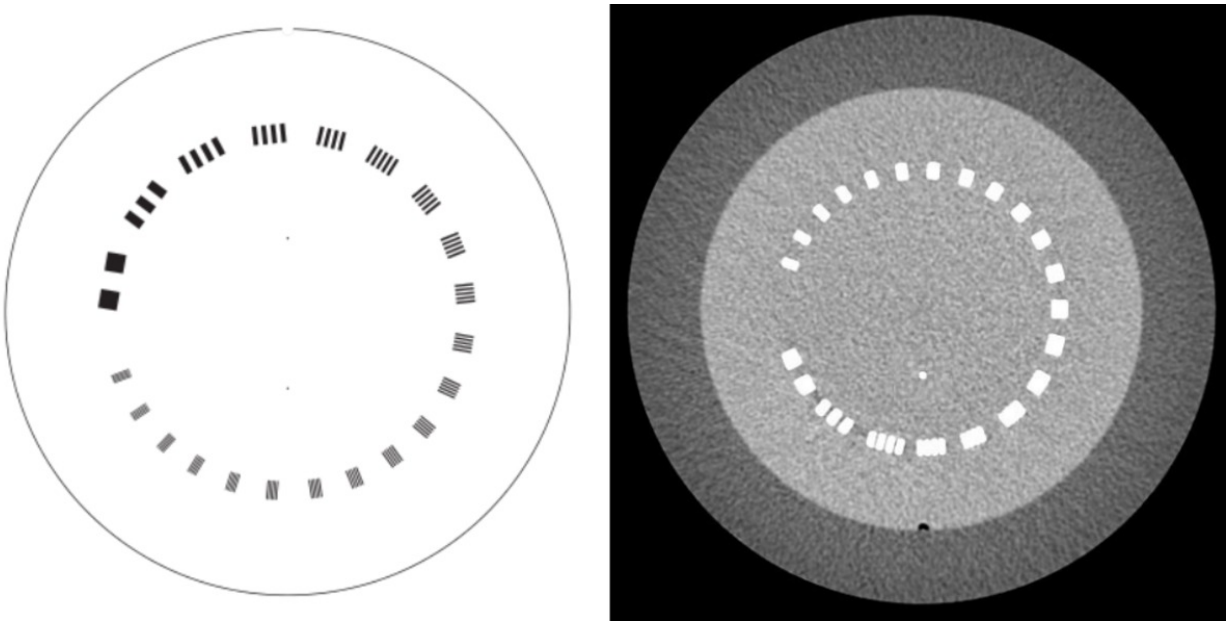

Fig. 4: Module CTP528 of the Catphan 504 phantom.

© - Pisa/IT

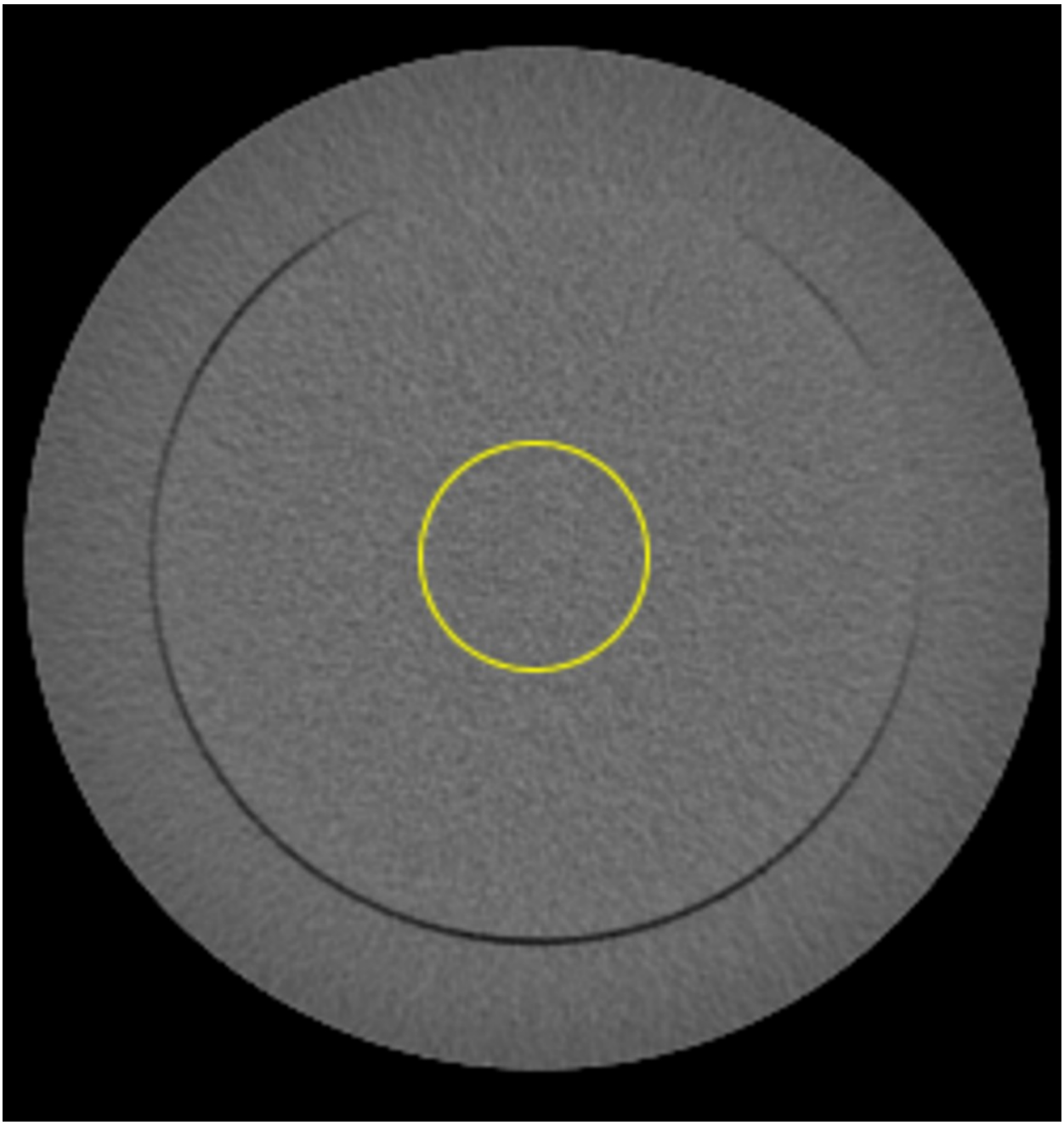

Fig. 5: ROI used for SD calculations.

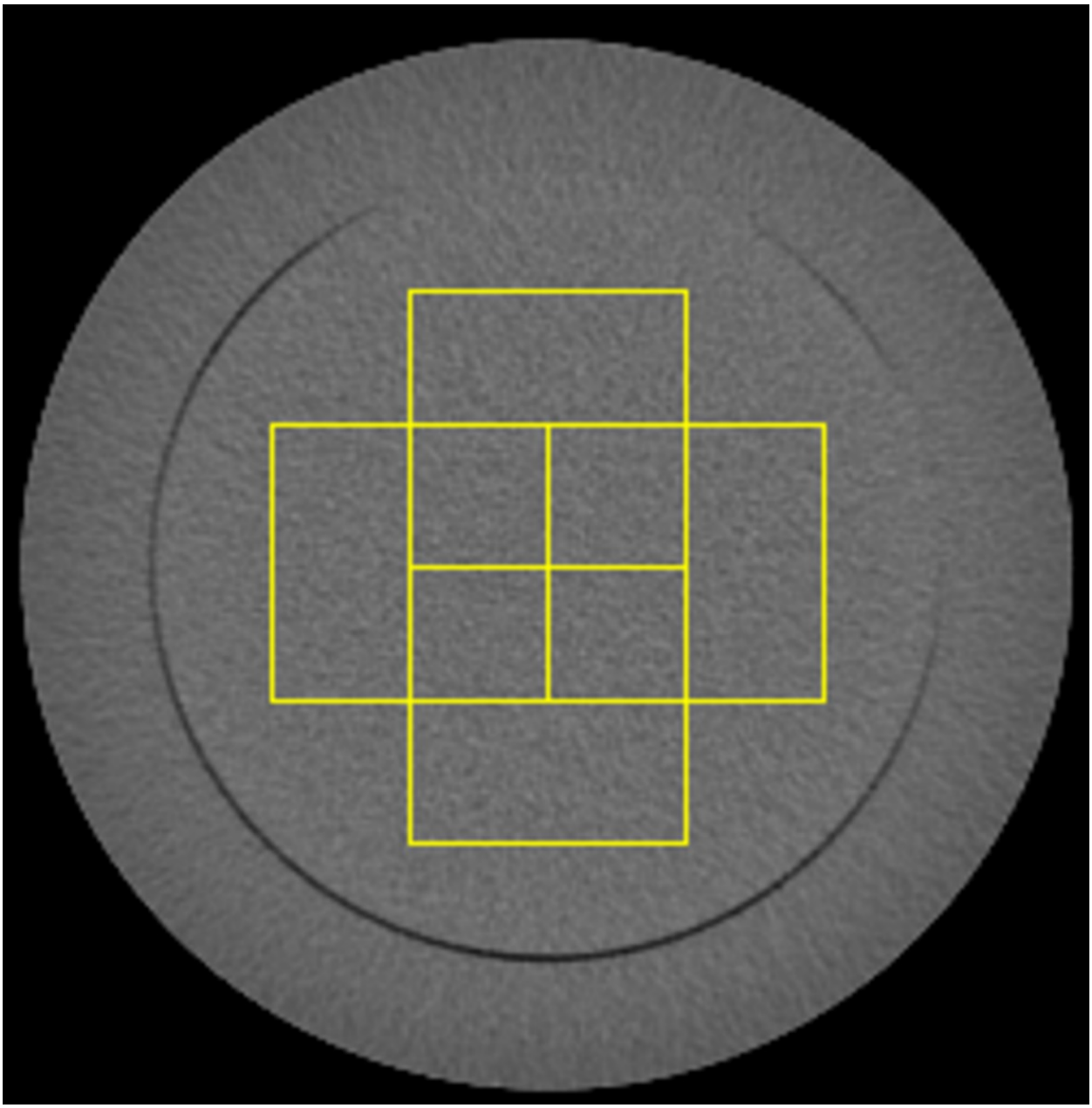

Fig. 6: ROI used for NPS calculations.

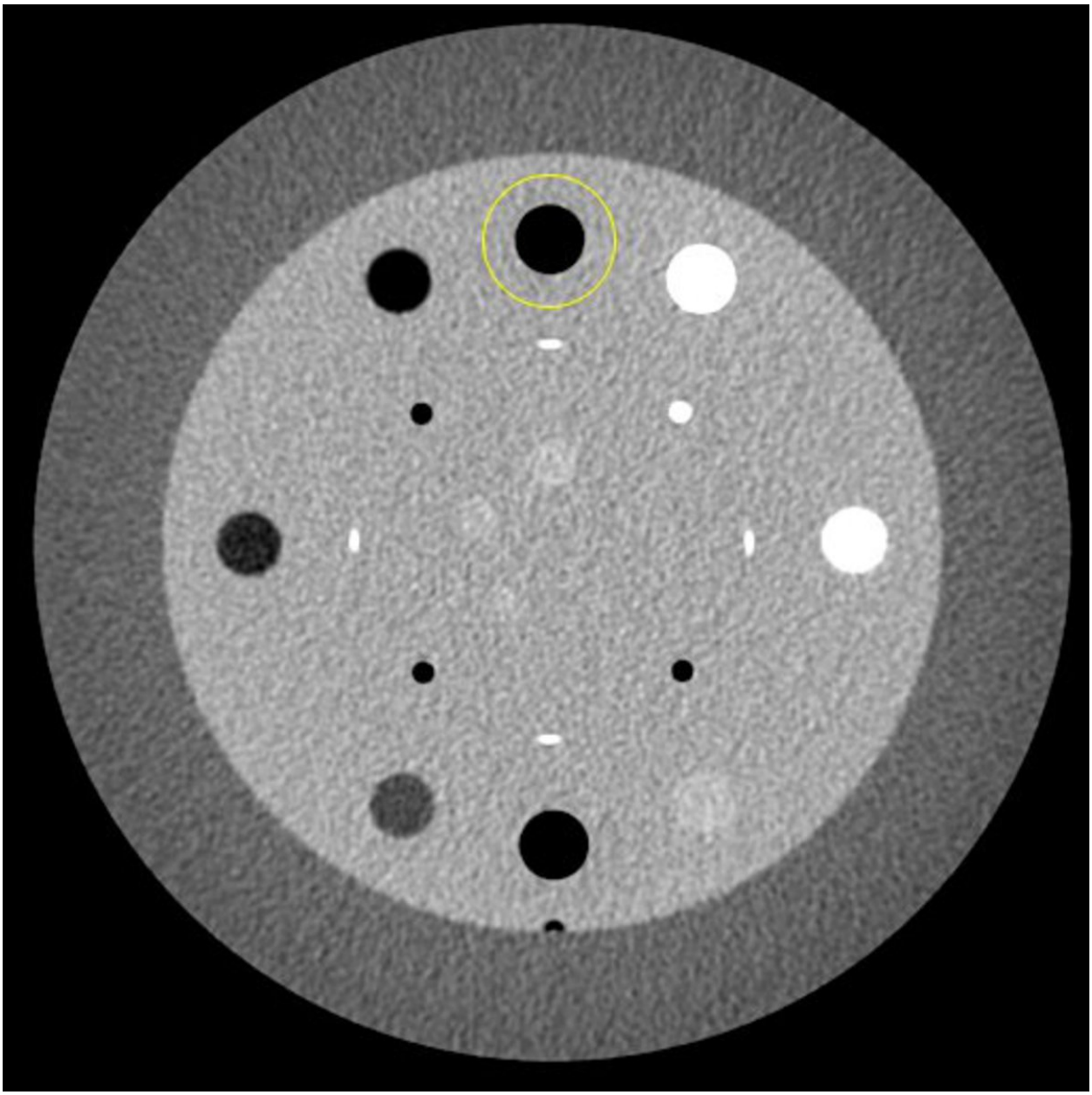

Fig. 7: ROI used for spatial resolution analysis with the circular edge method.

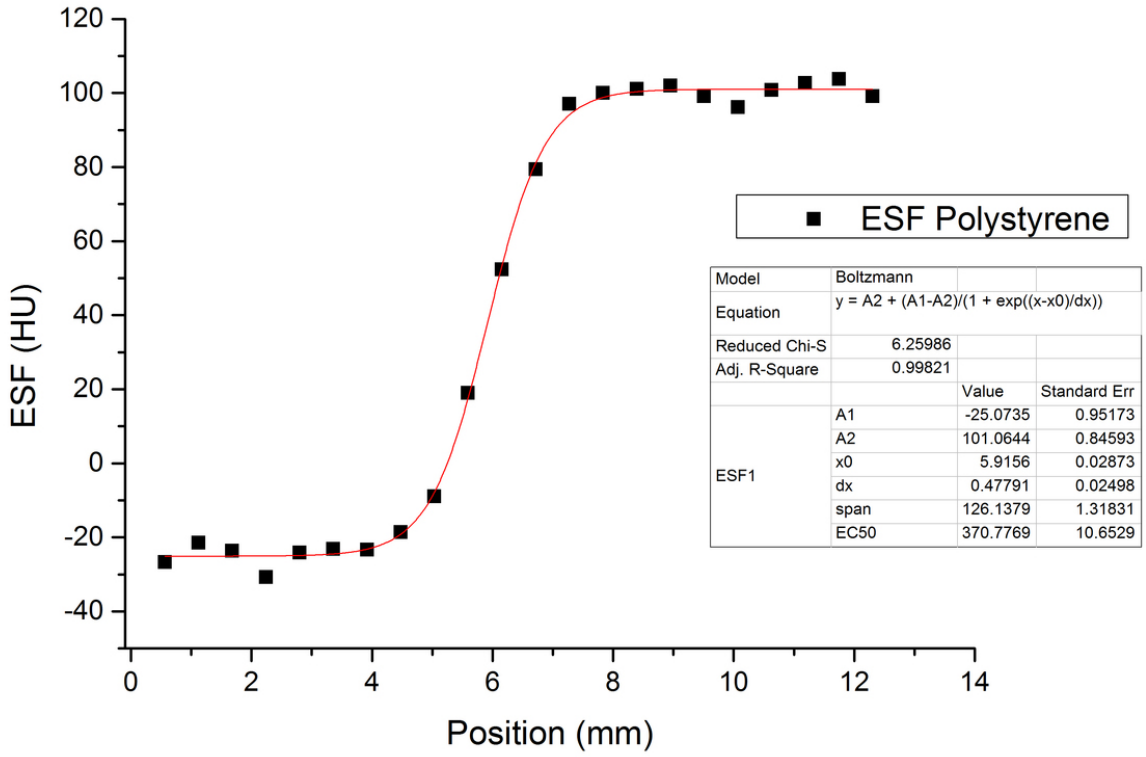

Model	Boltzmann		
Equation	y = A2 + (A1-A2)/(1 + exp((x-x0)/dx))		
Reduced Chi-S	6.25986		
Adj. R-Square	0.99821		
		Value	Standard Err
ESF1	A1	-25.0735	0.95173
	A2	101.0644	0.84593
	x0	5.9156	0.02873
	dx	0.47791	0.02498
	span	126.1379	1.31831
	EC50	370.7769	10.6529

Fig. 8: Example of edge spread function computed from the Polystyrene insert of the CTP404 module.

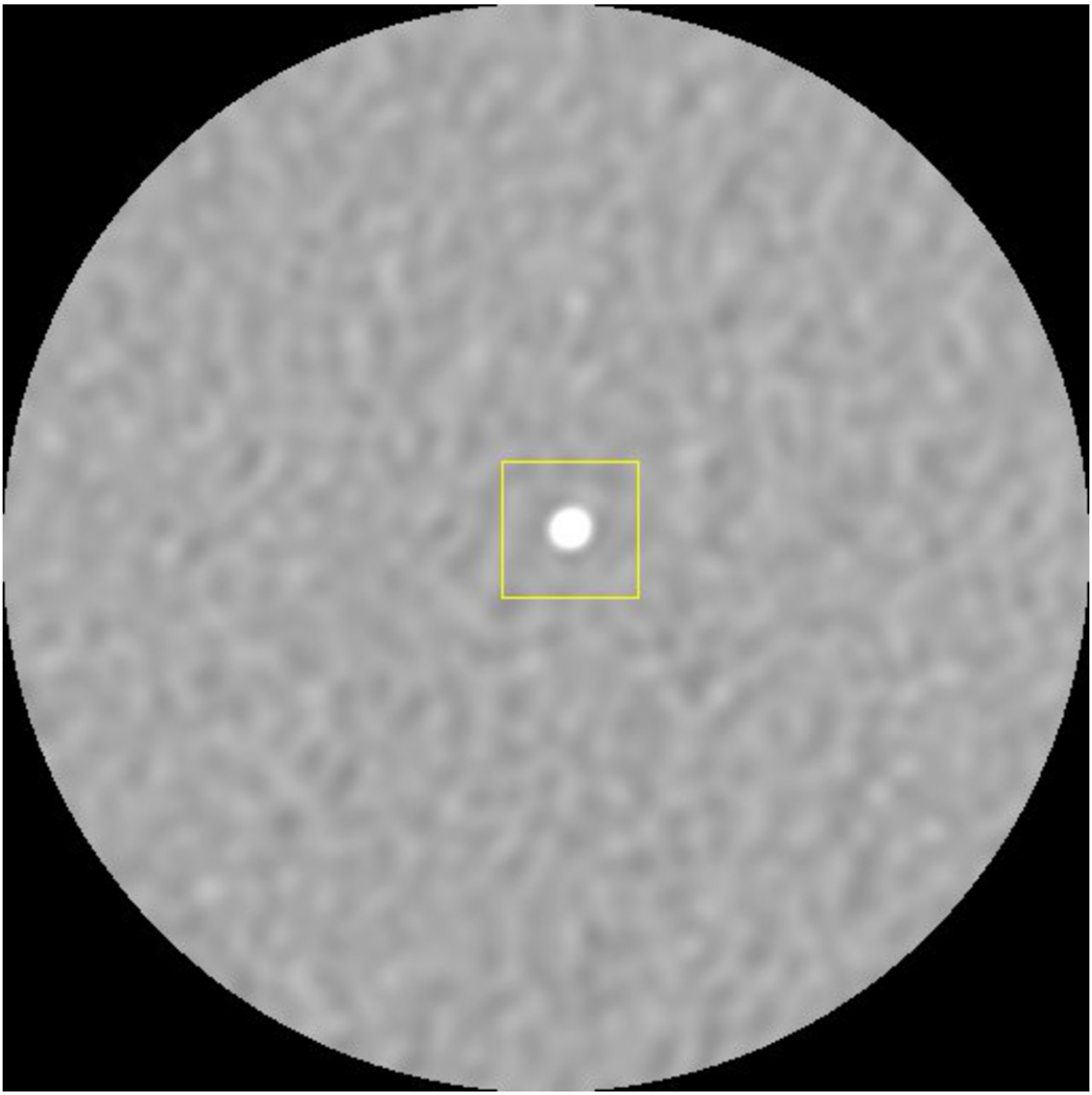

Fig. 9: Image of the 0.28 mm diameter bead (CTP528 module) used to evaluate the PSF of the system.

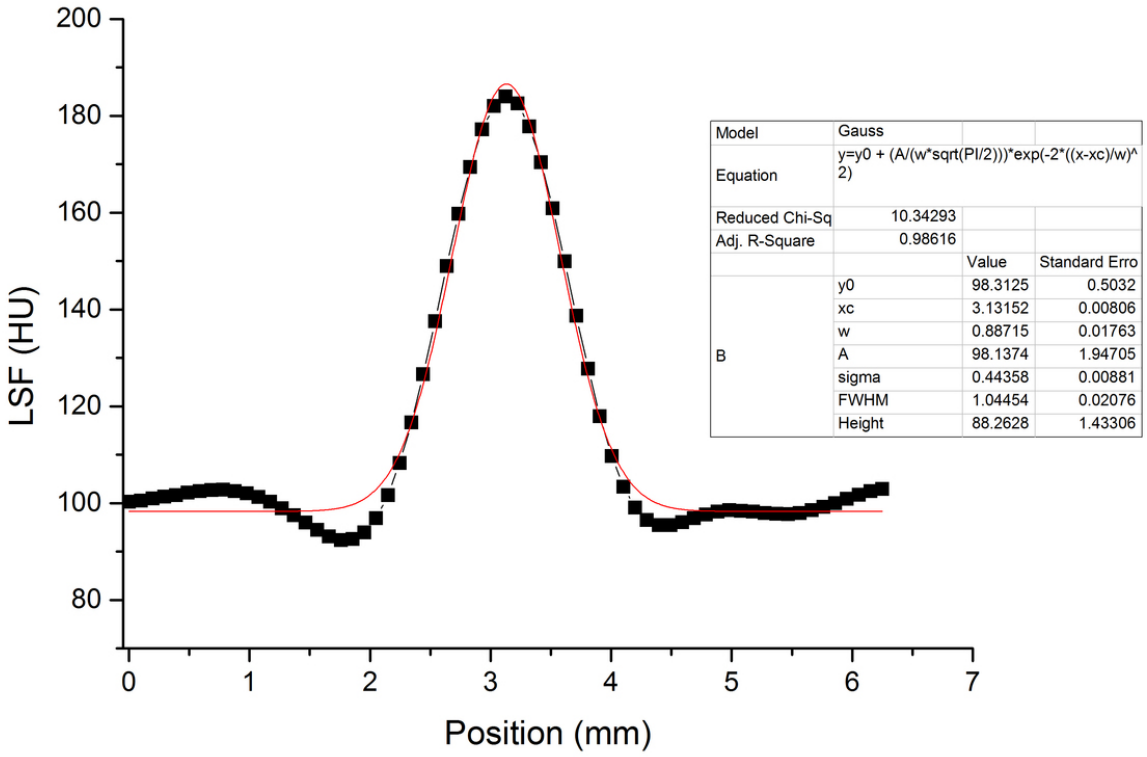

Fig. 10: Example of LSF.

Results

1) Noise

SD analysis

Fig. 11 on page 23 to Fig. 14 on page 26 show the SD values as a function of mAS, kV, slice thickness and pitch for different ASIR percentages of reconstruction.

According to the Poisson statistical model of the image noise, when mAs, kV and slice thickness increase, the image noise decreases since more photons contribuite to image formation. On the contrary, increasing pitch leads to an increase of noise since less x-ray quanta contribuite to the image formation.

As expected, increasing the ASIR percentage of reconstruction leads to a gradual reduction of the SD value (up to about 50%) without modifying the noise dependence from the considered scanning parameters. The maximum noise reduction, with respect to FBP, is obtained using ASIR 100%.

NPS analysis

In Fig. 15 on page 27 we show two examples of noise texture and magnitude from FBP-reconstructed images and ASIR 100% -reconstructed images acquired at 28 mAs and 224 mAs and using the others paramer values shown in Tab. 2a. The noise reduction is accompained by an evident change in the noise texture, particularly for high percentages of ASIR recontruction.

An example of 3D-NPS calculation along fz=0, fx=0 and fy=0 is shown in Fig. 16 on page 28. The example compares FBP and ASIR 100% reconstructions. The maximum spatial frequency value was obtained by considering Nyquist sampling creiterion. From Fig. 16 on page 28 we can see that ASIR 100% reduces the image noise mostly at high spatial frequency. To allow a good visualization of NPS calculated from ASIR reconstruction, the brightness level was artificially enhanced with respect to NPS calculated from FBP reconstruction (the original NPS images were too dark at the same brightness level since the considerable noise reduction performed by ASIR). This behaviour is more clearly expressed in Fig. 17 on page 29, which plots the radial average of 3D-NPS along fz=0 for different ASIR percentages of reconstruction. Fig. 17 on page 29 shows the shape of NPS curves obtained with FBP and ASIR (20% to 100%) reconstructions: by increasing ASIR precentage of reconstruction there is a non-

uniform reduction in NPS curve values with respect to FBP reconstruction. In fact, the reduction of noise is observable especially at high spatial frequency.

The 2D-NPS calculations, for different ASIR precentages of reconstruction, are shown in Fig. 18 on page 30. Like the 3D-NPS along fz=0, the 2D NPS exhibit a radial simmetry that indicates that the detection of an object does not depend significantly on its orientation with respect to the image axial plane. A radial average of 2D NPS gives the NPS curves (shown in Fig. 19 on page 31) and confirm the changes in NPS curve shapes introduced by ASIR recntruction that appears in Fig. 17 on page 29. Note that in the 2D case the ensamble of ROI was composed of only 5 ROI, thus a noisy curve shape is expected compared to the 3D (along fz=0) case of Fig. 17 on page 29, in which the ensamble of VOI was composed of 20 VOI.

From Fig. 17 on page 29 we can see that, by increasing the ASIR percentage of reconstruction, the peak of the NPS curve moves from approximately 0.30 mm^{-1} (i.e. spatial dimensions of about 1.7 mm) for FBP reconstruction, to 0.15 mm^{-1} (i.e. spatial dimensions of about 3.3 mm) for ASIR 100% reconstruction.

These results are in agreement with what is shown in previous works [4, 12] and confirm the changes in the NPS for different ASIR percentages compared to the conventional FBP.

2) Spatial resolution

Fig. 20 on page 32 - Fig. 22 on page 33 show plots of the MTF calculated from FBP-, ASIR 60%- and 100%-reconstructed images, acquired at 28 mAs and 224 mAs (lowest and highest mAs value used) for different contrast levels. Fig. 20 on page 32 also plots the MTF measured with the PSF method.

For FBP-reconstructed images, as expected, the MTF exhibits a substantial independence from the contrast (see Fig. 20 on page 32). Also note the agreement between the circular edge method and the PSF method (verification method). Contrariwise, for ASIR-rconstructed images the MTF is contrast-dependent (Fig. 21 on page 32 and Fig. 22 on page 33) and this is true especially for high ASIR percentages of reconstruction and for low mAs values. In particular, the MTF worsens when contrast decreases and this behaviour appears clearer in Fig. 22 on page 33 by considering the CT HU of Tab. 1 (i.e. contrast decreases from air- to polystyrene-background).

Fig. 23 on page 33 and Fig. 24 on page 34 show the MTF curves calculated from FBP- and ASIR 100%-reconstructed images for Air and Polystyrene inserts (highest and lowest constrasts in CTP404 module) at various mAs values.

The MTF calculated from FBP-reconstructed images across the wide range of mAs considered results in agreement for all mAs values within the uncertainties (Fig. 23 on page 33). On the other hand, for ASIR-reconstructed images, the MTF calculated for low-contrast inserts (e.g. Polystyrene, Fig. 24 on page 34) shows lower values for low mAs acquisitions. This behaviour is more evident for high percentages of ASIR and indicates that the MTF for ASIR-reconstructed images is dose-dependent.

To directly appreciate the comparison between MTF calculations from FBP and ASIR reconstruction, in Fig. 25 on page 34 - Fig. 27 on page 36 we plotted the MTF calculated from FBP- and ASIR-reconstructed images, acquired at the lowest mAs value (28 mAs), for the Air (highest contrast in CTP404 module), LDPE and Polystyrene (lowest contrast in CTP404 module) inserts.

In Fig. 25 on page 34 we can see that the MTF curves computed for the Air insert are very close to each other and almost overlap, leading to a not appreciable difference between the FBP and ASIR reconstructions in terms of spatial resolution. However, for the medium-low contrast insert (LDPE), and especially for the lowest contrast insert (Polystyrene), incrasing the ASIR percentage of reconstruction leads to a worsening of the MTF, as we can appreciate in Fig. 26 on page 35 and Fig. 27 on page 36. In these cases, ASIR provides low performance in terms of spatial resolution compared to FBP.

As an example to summarize these results, in Fig. 28 on page 37 and Fig. 29 on page 38 we plotted the MTF values computed at a 0.51 mm^{-1} spatial frequency (i.e. spatial dimensions of about 1 mm) as a function of contrast (fixing the lowest mAs value) and mAs (fixing the lowest contrast level) for FBP and ASIR 100% reconstruction. The data trend in Fig. 28 on page 37 and Fig. 29 on page 38 underlines that, in low-contrast and low-mAs situations, ASIR could degrade spatial resolution with respect to FBP reconstruction.

Images for this section:

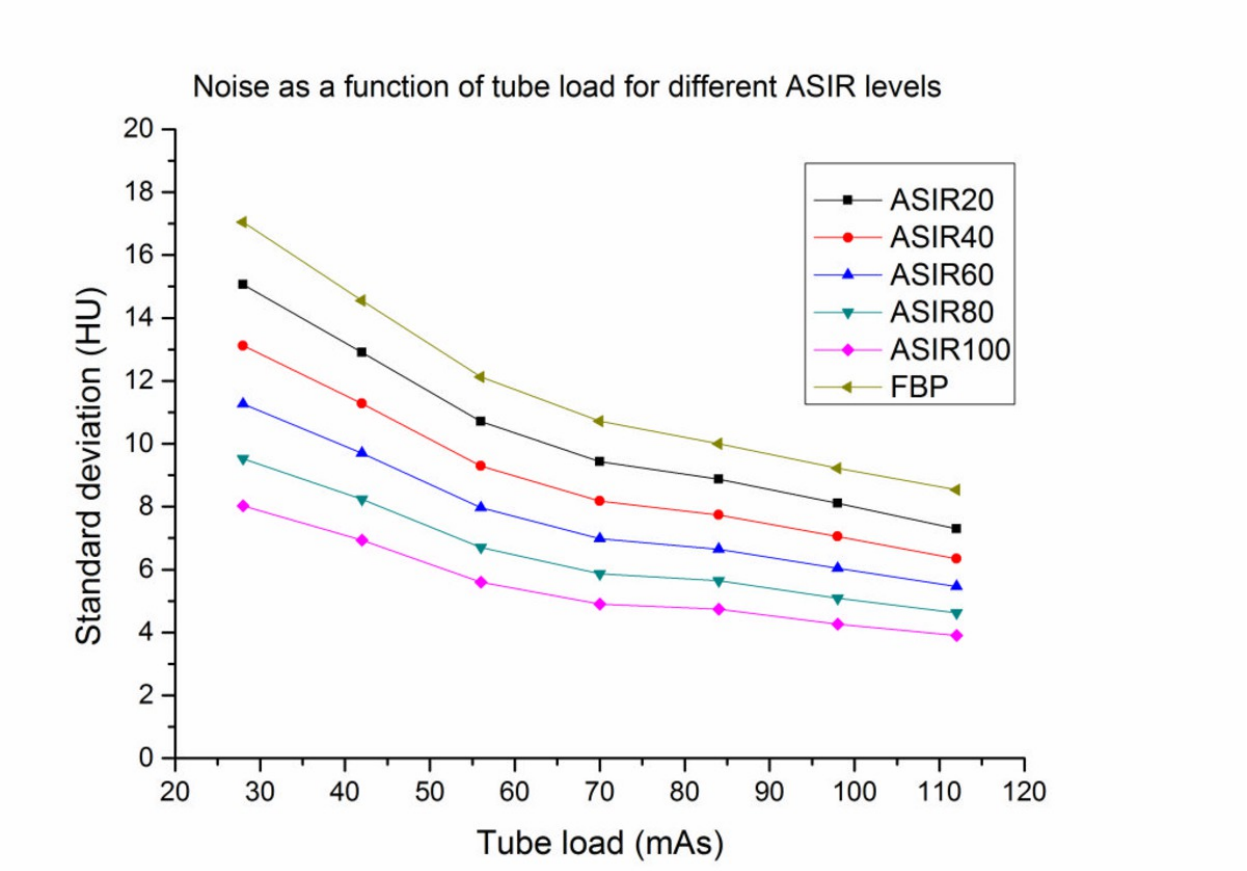

Fig. 11: Noise as a function of tube load.

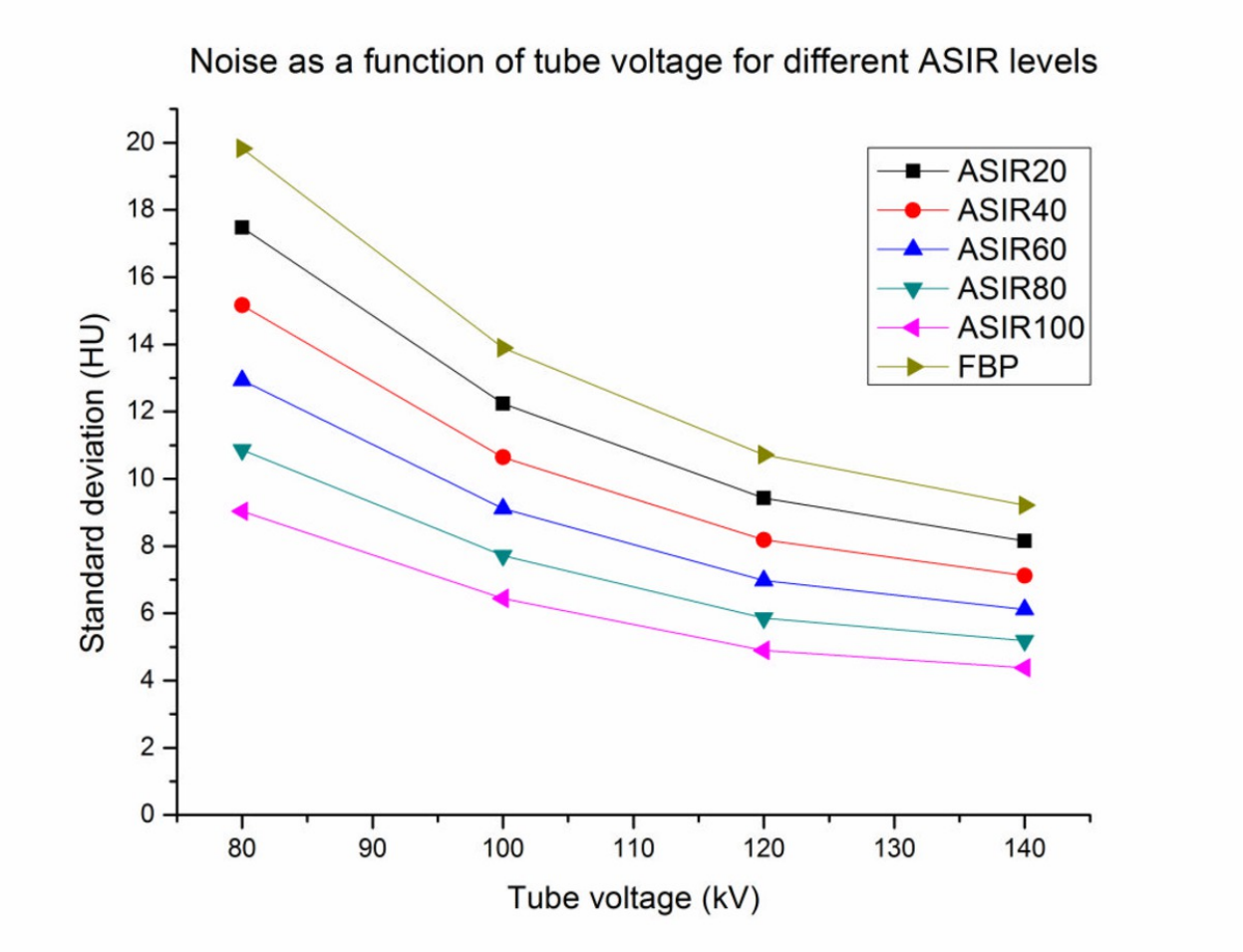

Fig. 12: Noise as a function of tube voltage.

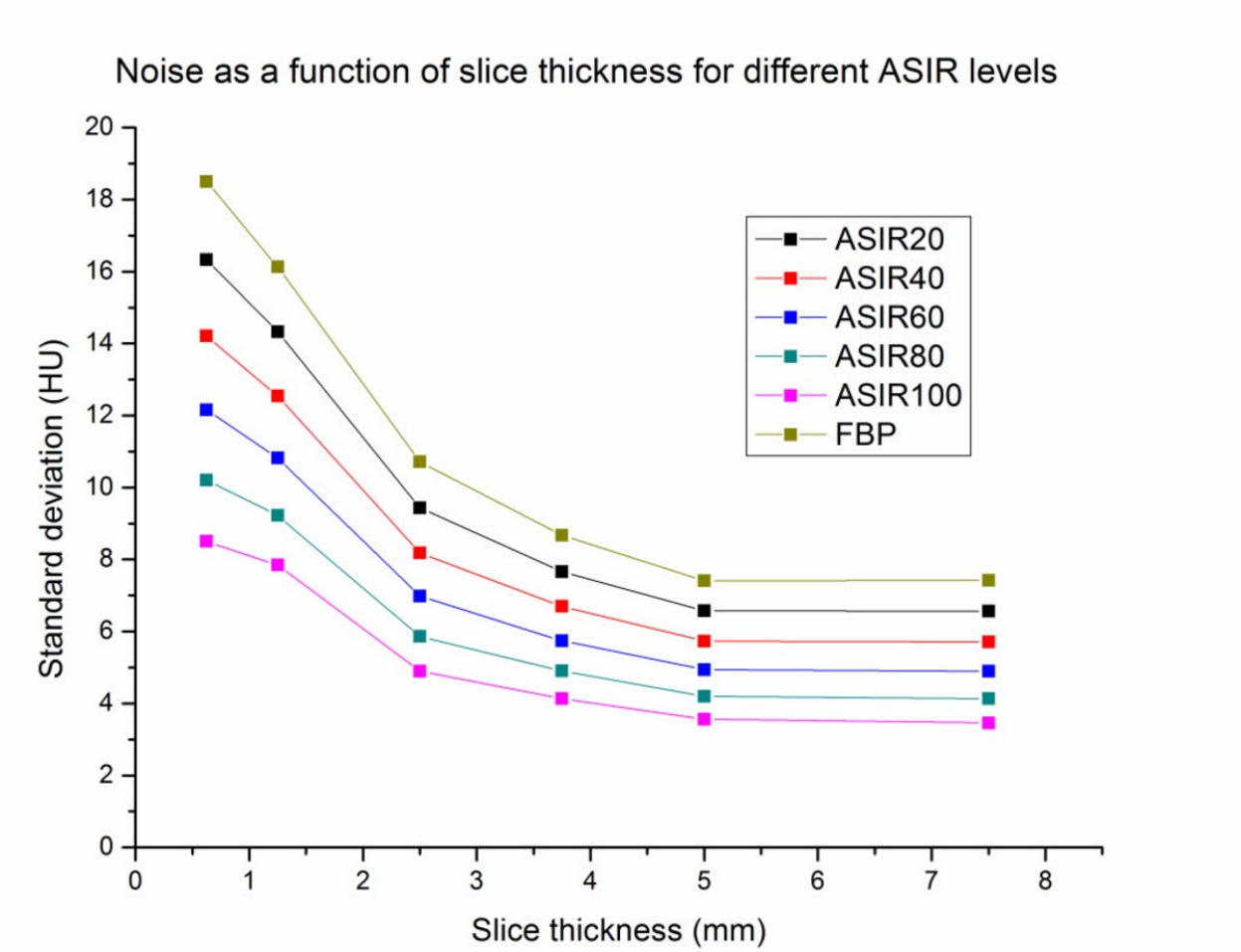

Fig. 13: Noise as a function of slice thickness.

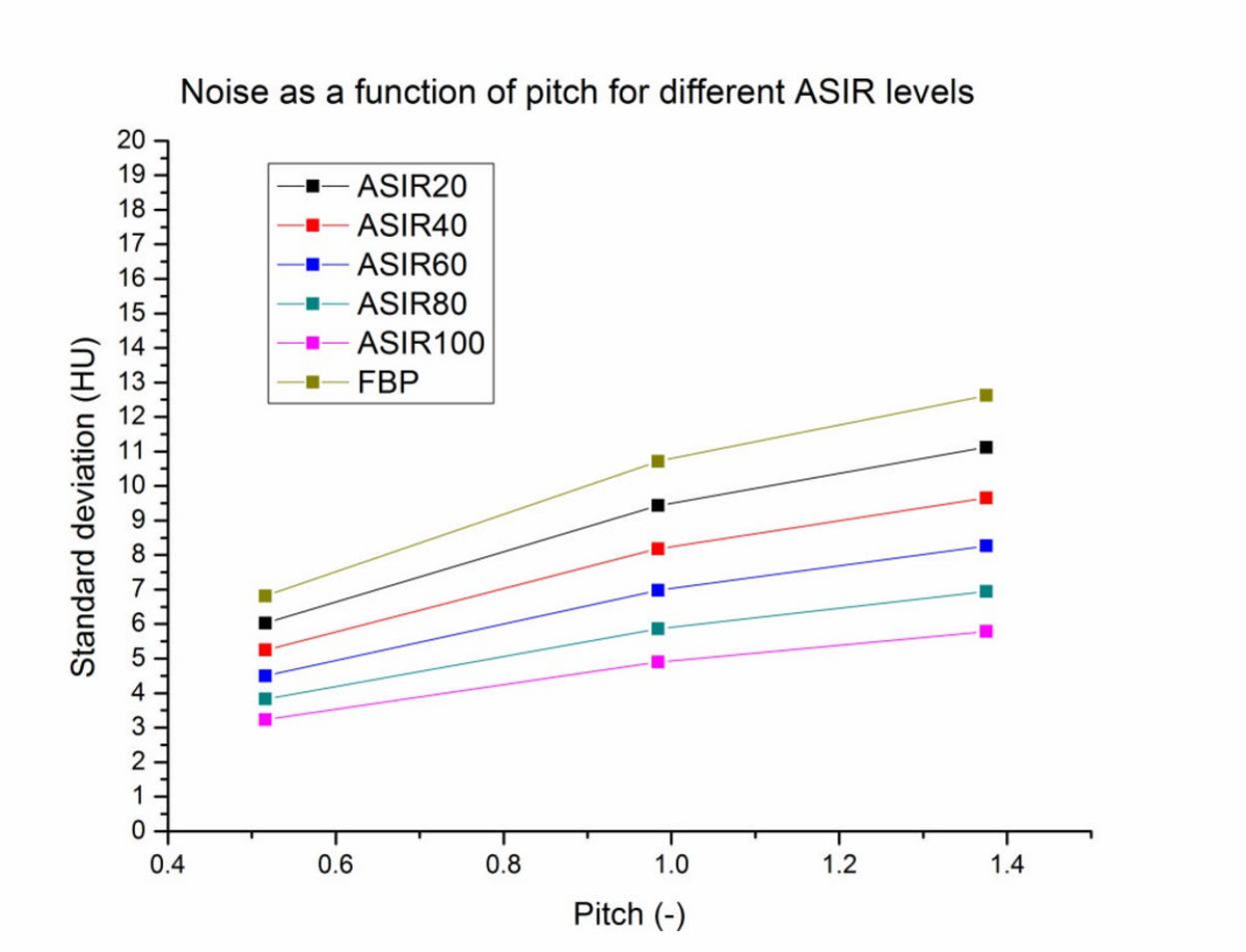

Fig. 14: Noise as a function of pitch.

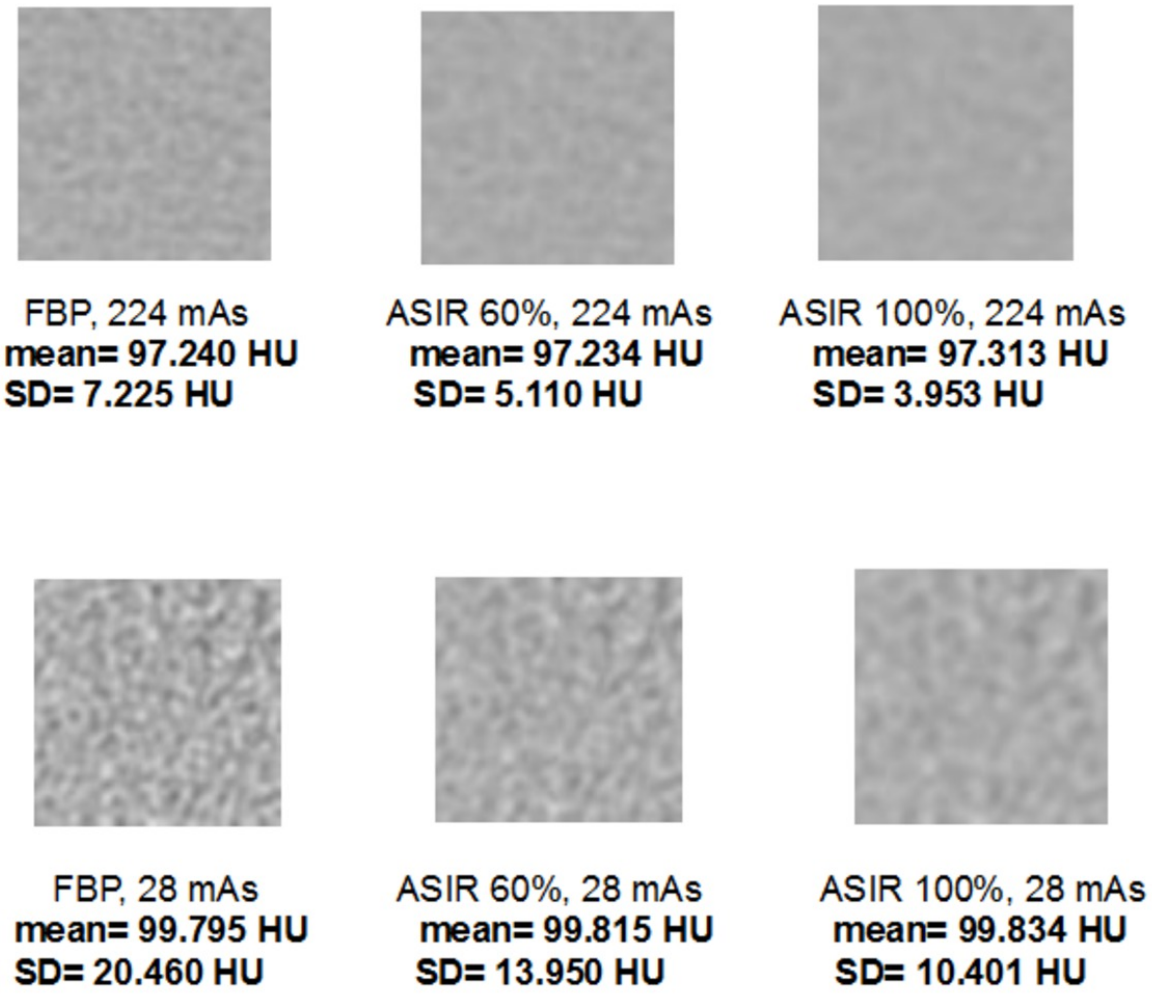

Fig. 15: Examples of noise textures at different ASIR levels of reconstruction.

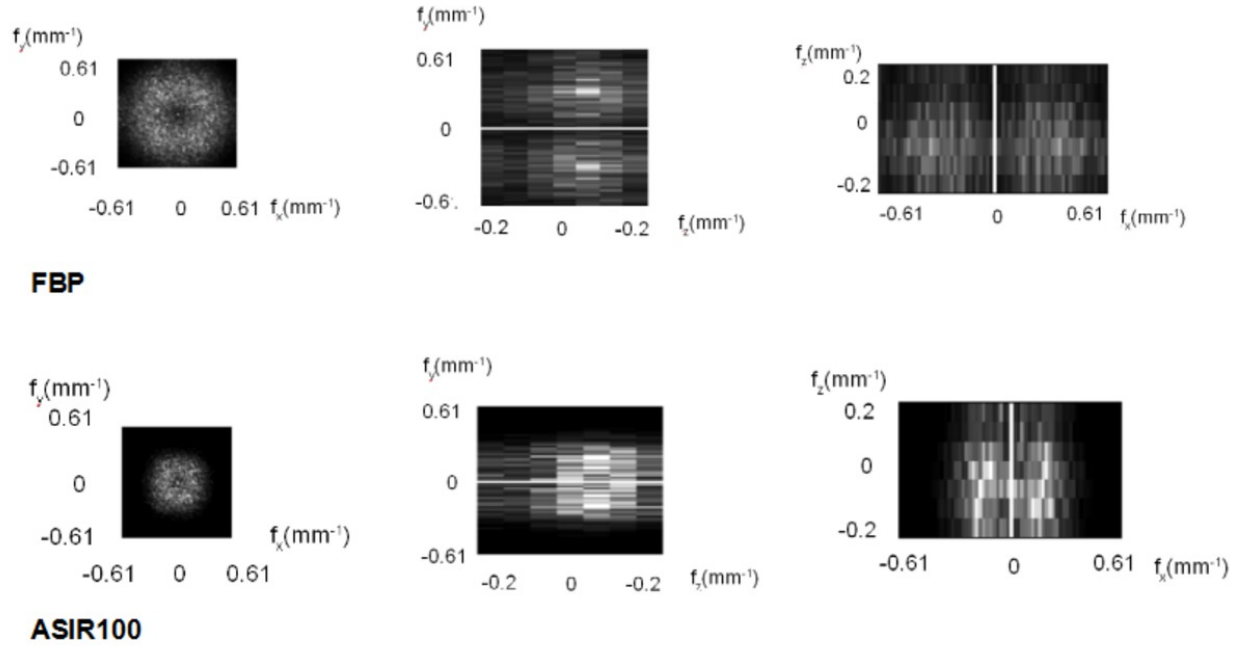

Fig. 16: Examples of (fx,fy), (fz,fy) and (fx,fy) planes of the 3D NPS.

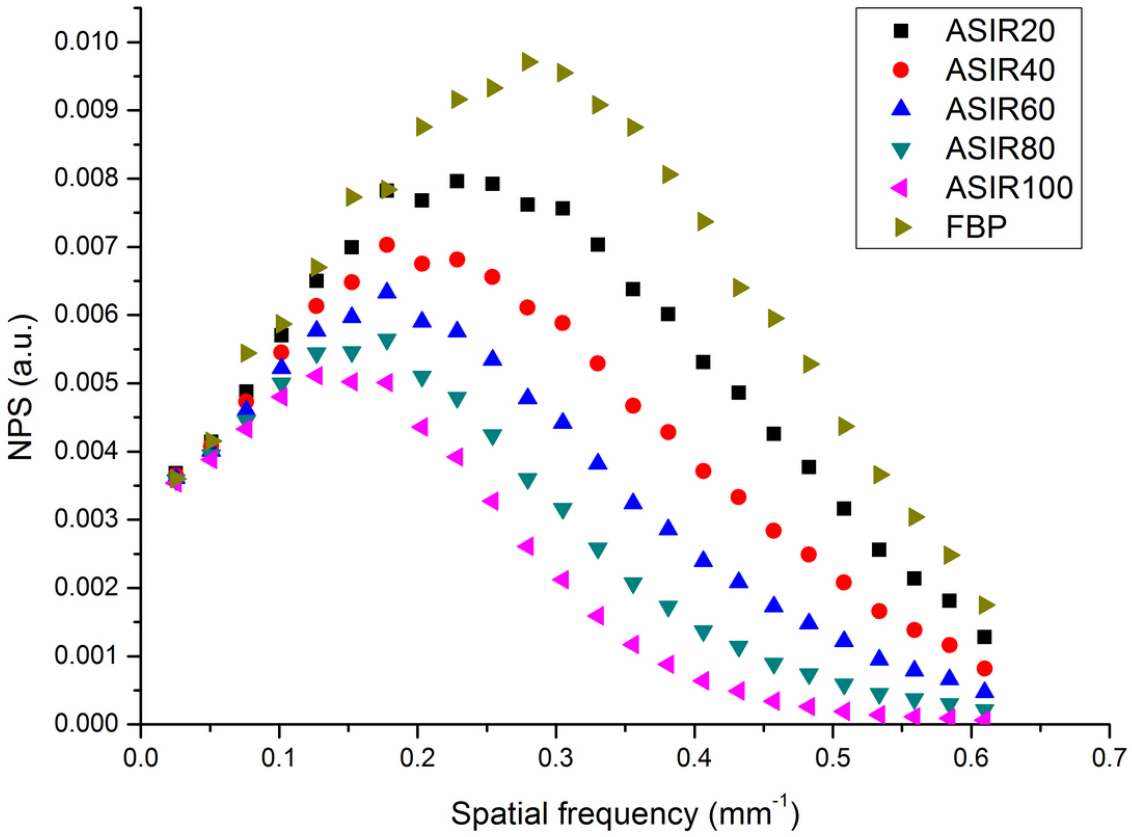

Fig. 17: Radial average of the 3D NPS along fz=0 (i.e. in (fx,fy) plane).

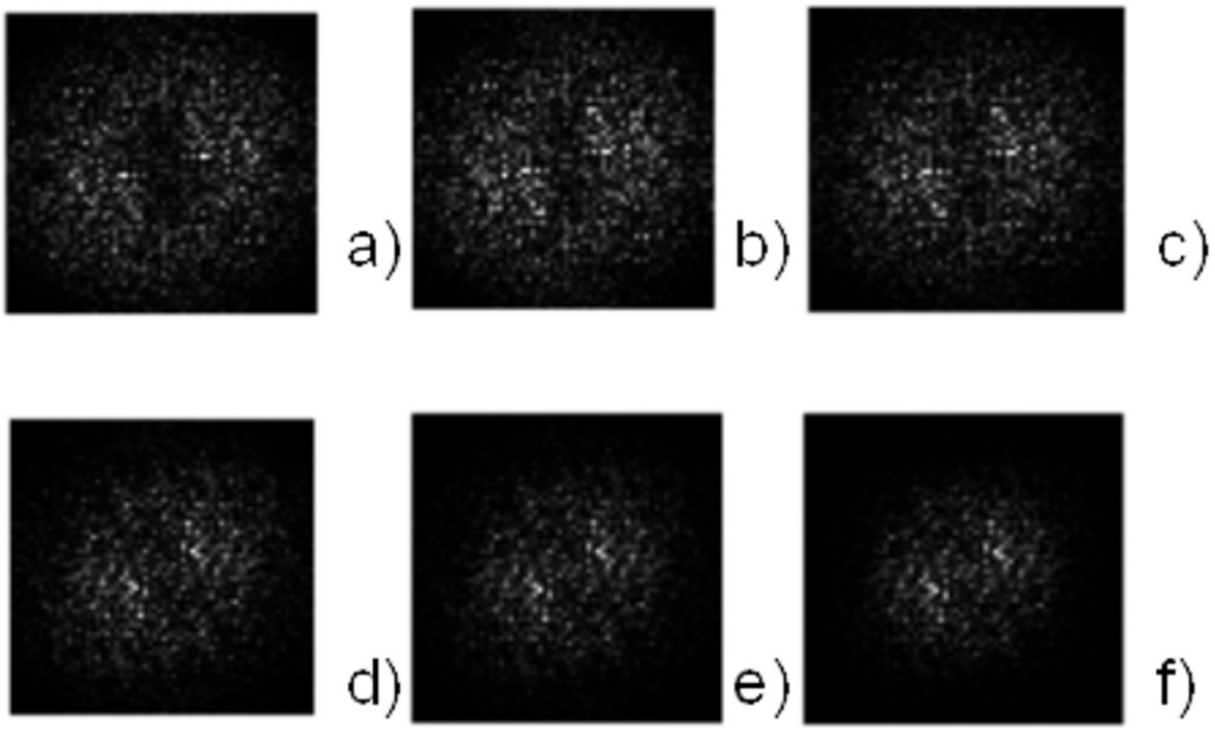

Fig. 18: 2D NPS for different ASIR reconstruction levels: a) FBP; b) ASIR 20%; c) ASIR 40%; d) ASIR 60%; e) ASIR 80%; f) ASIR 100%.

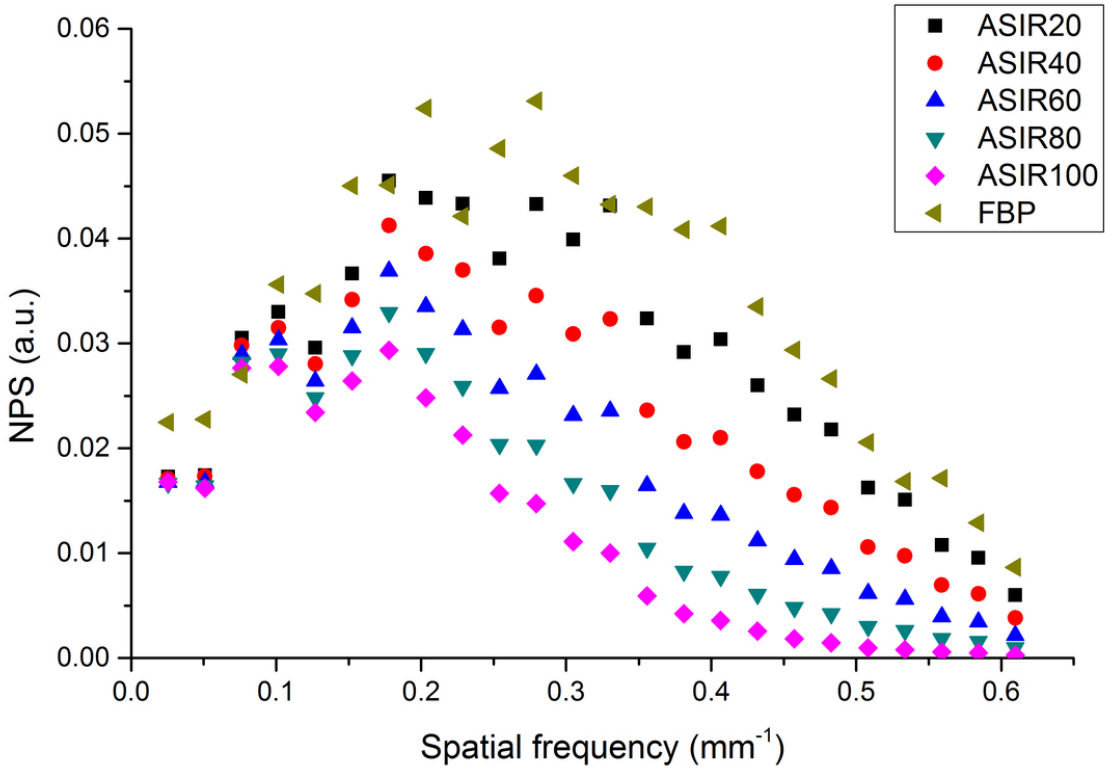

Fig. 19: Radial average of the 2D NPS.

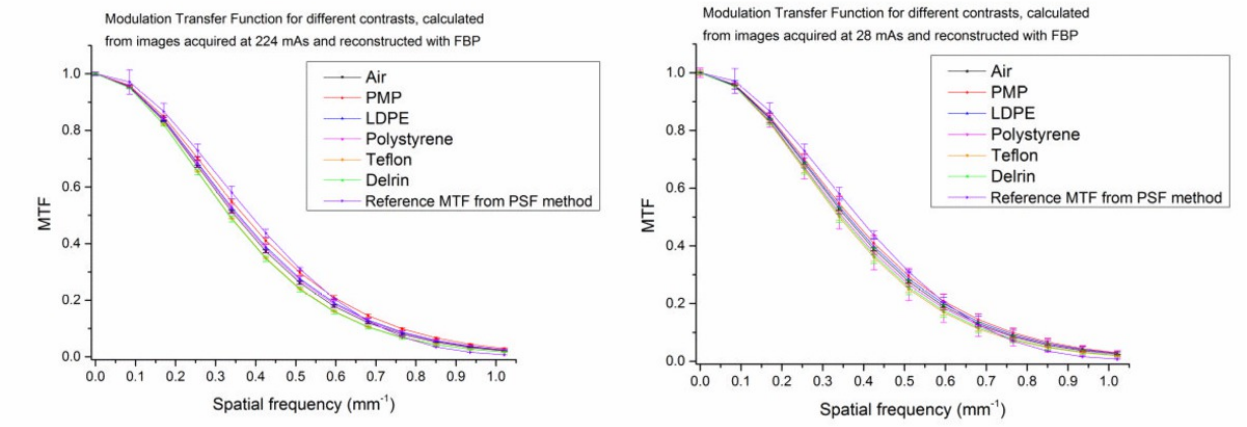

Fig. 20: MTF for different contrasts computed from images reconstructed with conventional FBP algorithm.

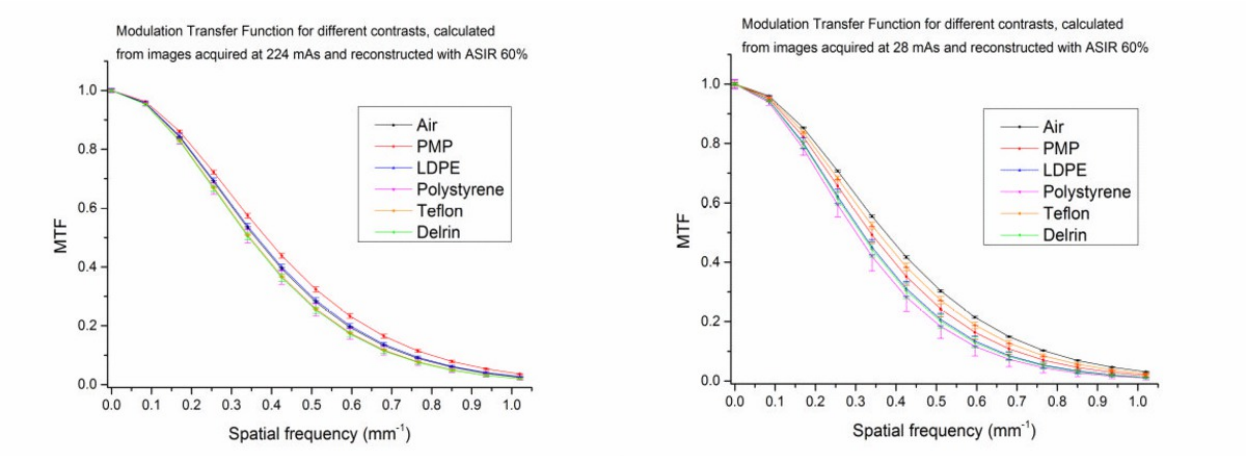

Fig. 21: MTF for different contrasts computed from images reconstructed with ASIR 60%.

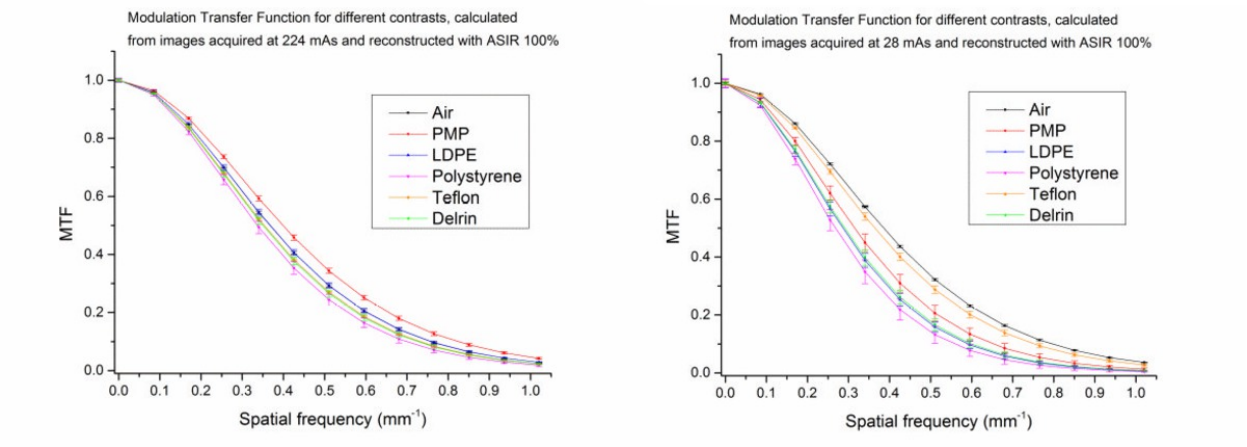

Fig. 22: MTF for different contrasts computed from images reconstructed with ASIR 100%.

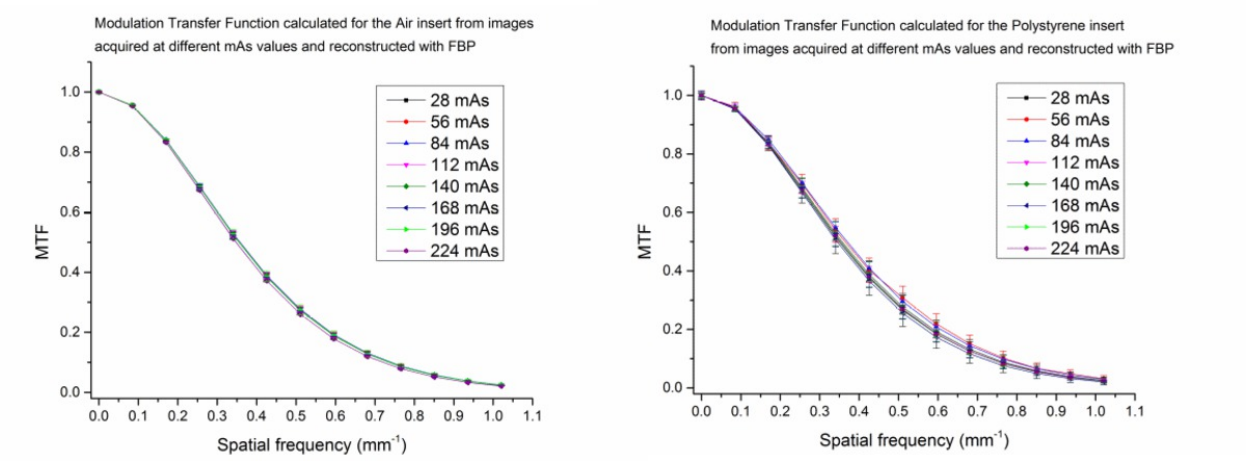

Fig. 23: MTF for different mAs values computed from images reconstructed with FBP.

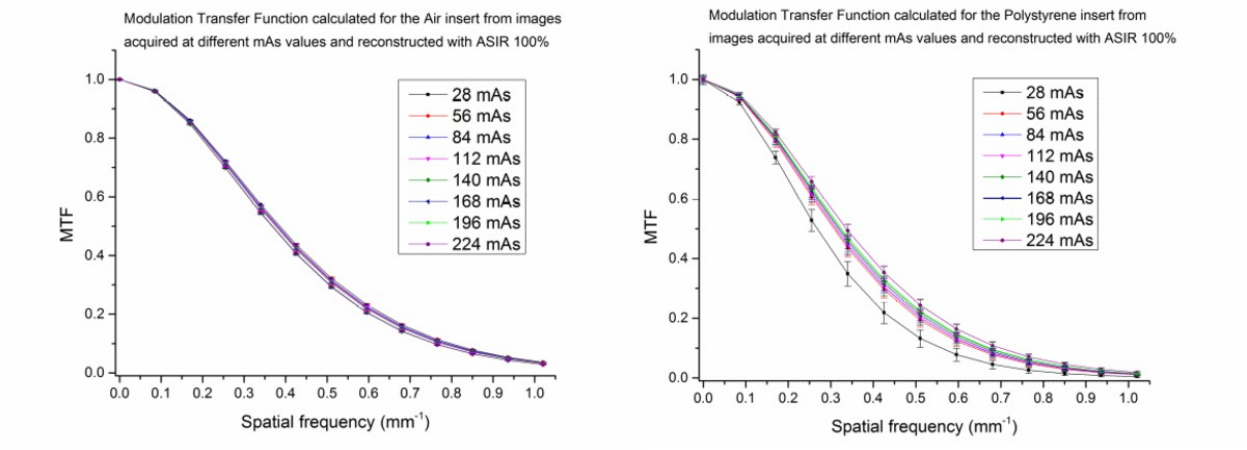

Fig. 24: MTF for different mAs values computed from images reconstructed with ASIR 100%.

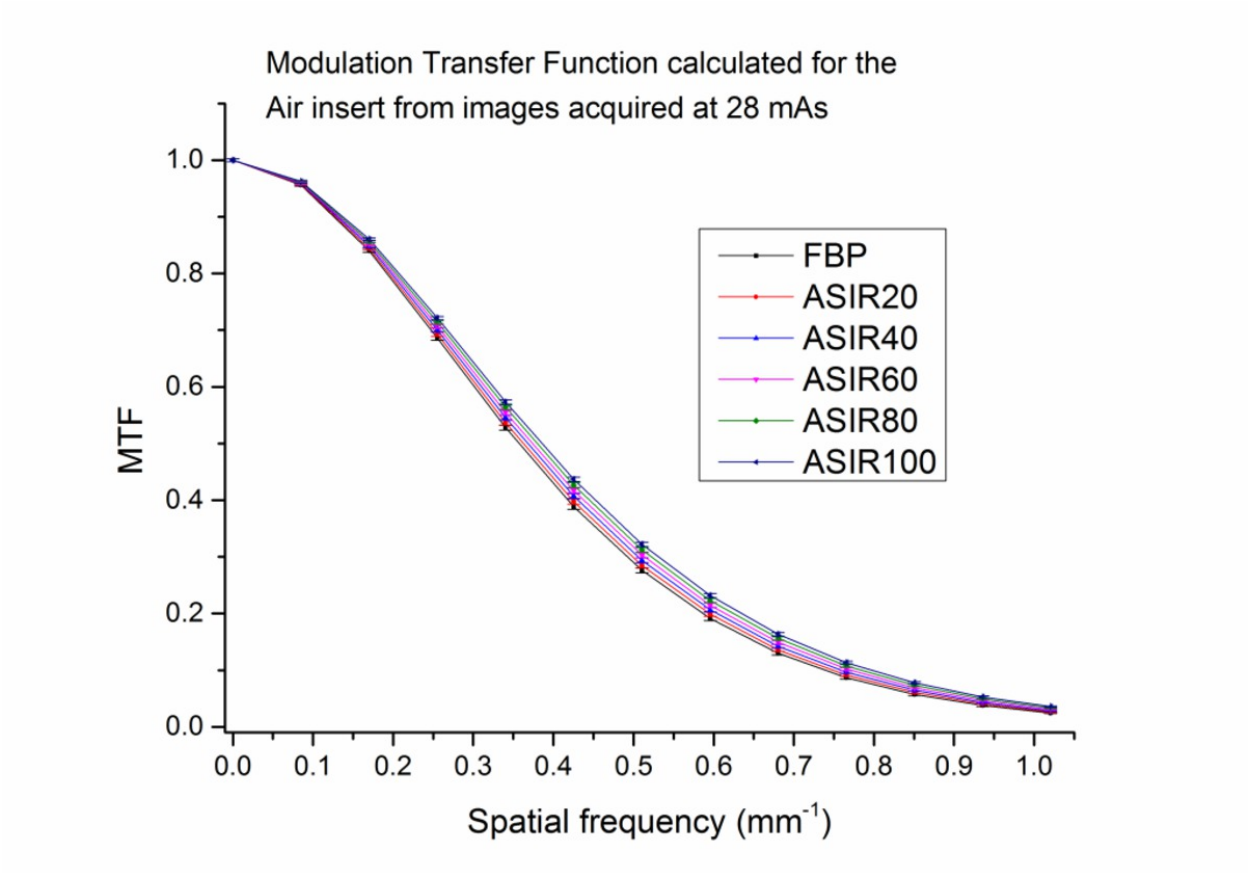

Fig. 25: MTF calculated for the Air insert at different ASIR reconstruction levels.

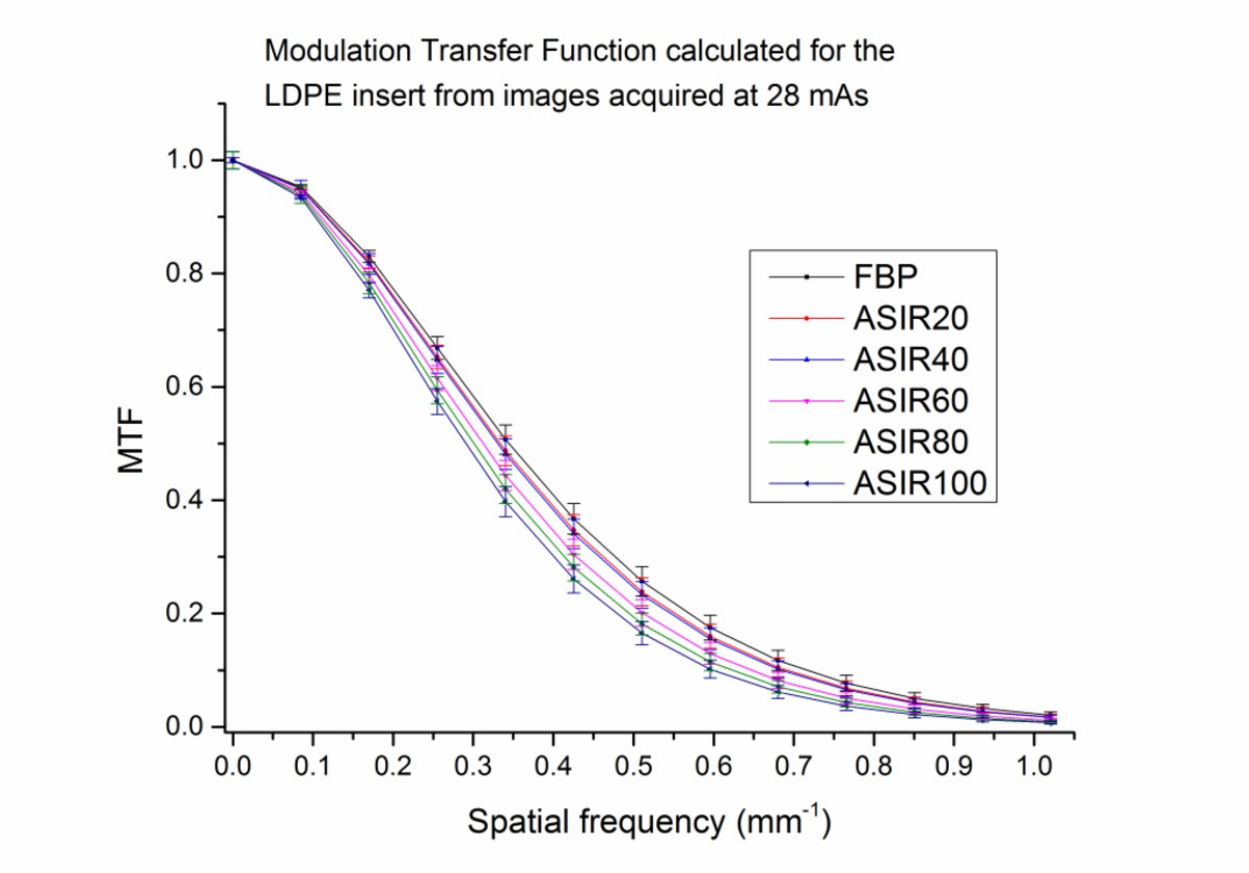

Fig. 26: MTF calculated for the Air insert at different ASIR reconstruction levels.

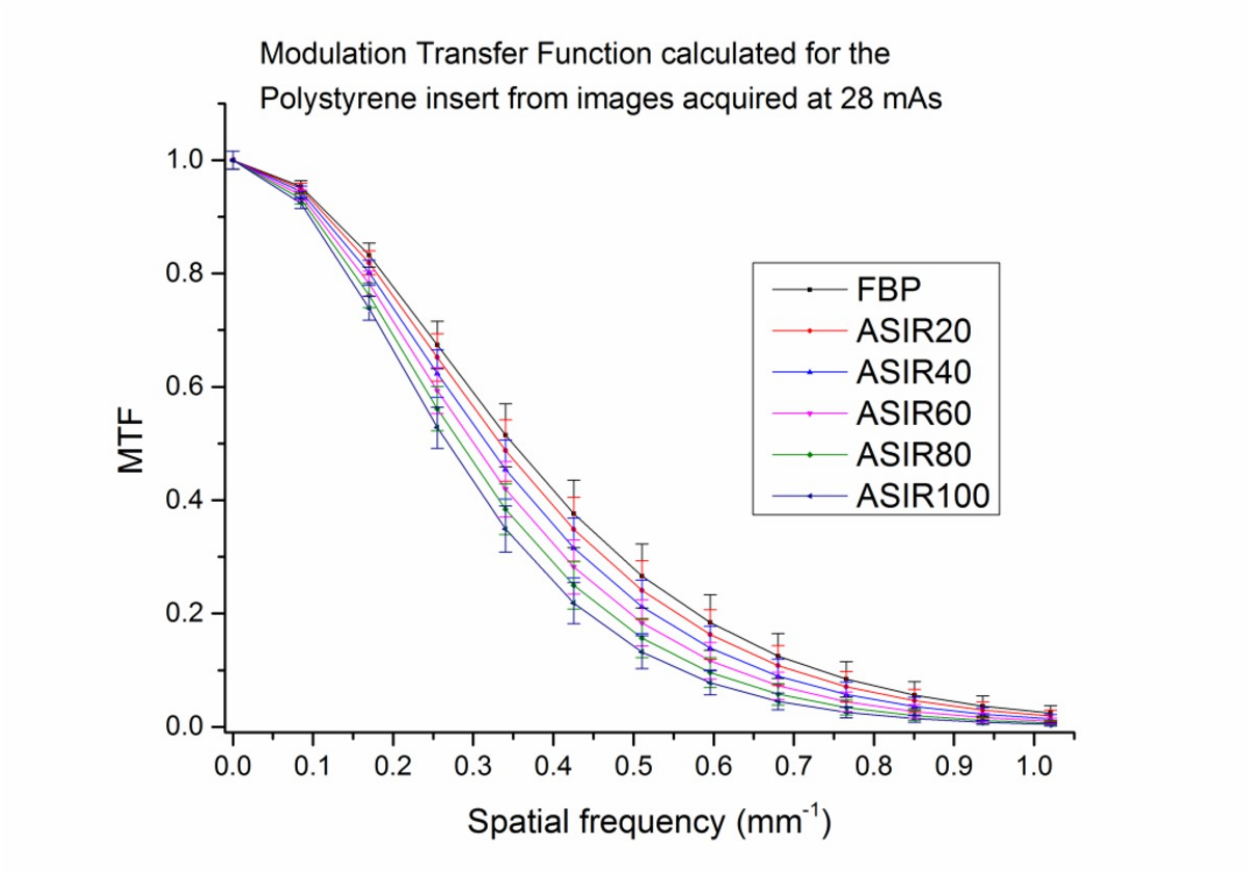

Fig. 27: MTF calculated for the Air insert at different ASIR reconstruction levels.

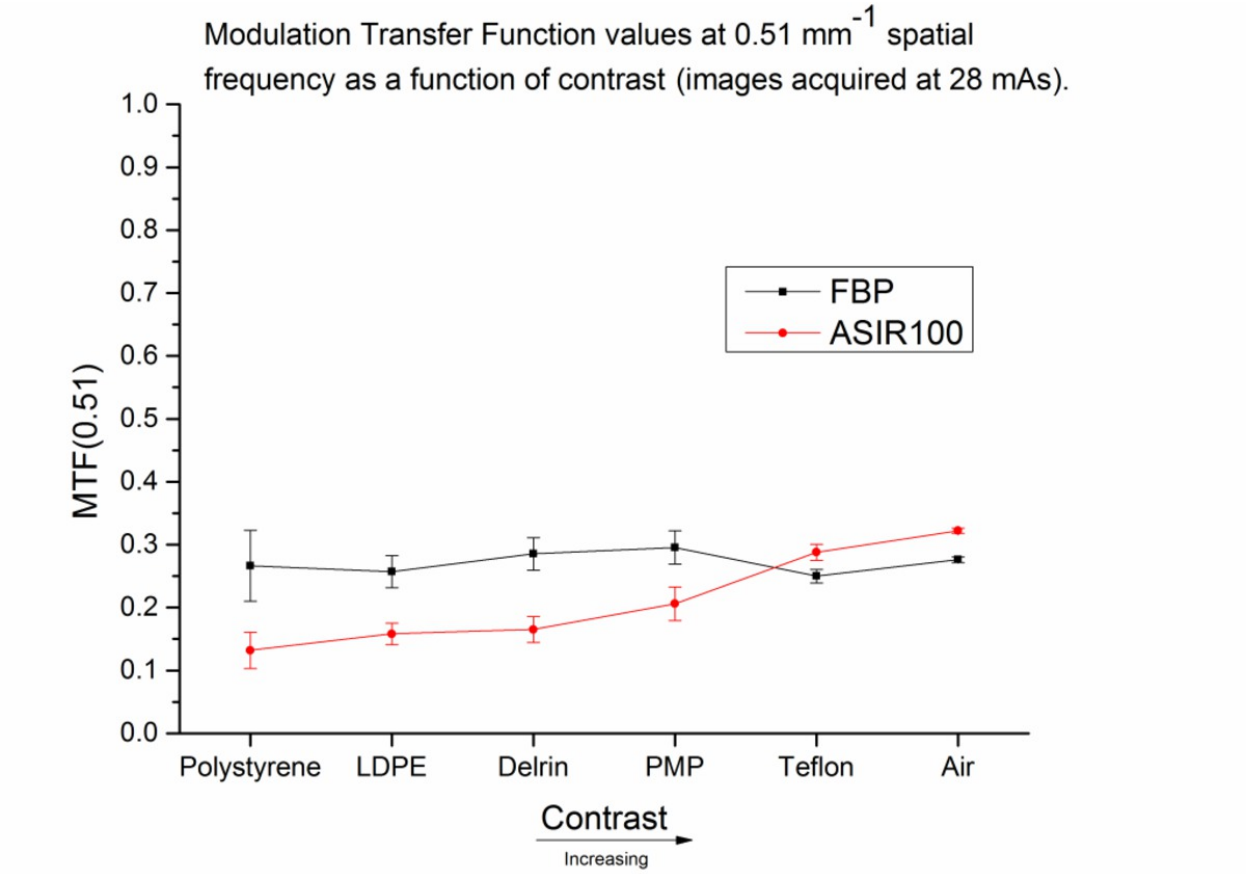

Fig. 28: MTF values at 0.51 mm^-1 spatial frequency as a function of contrast.

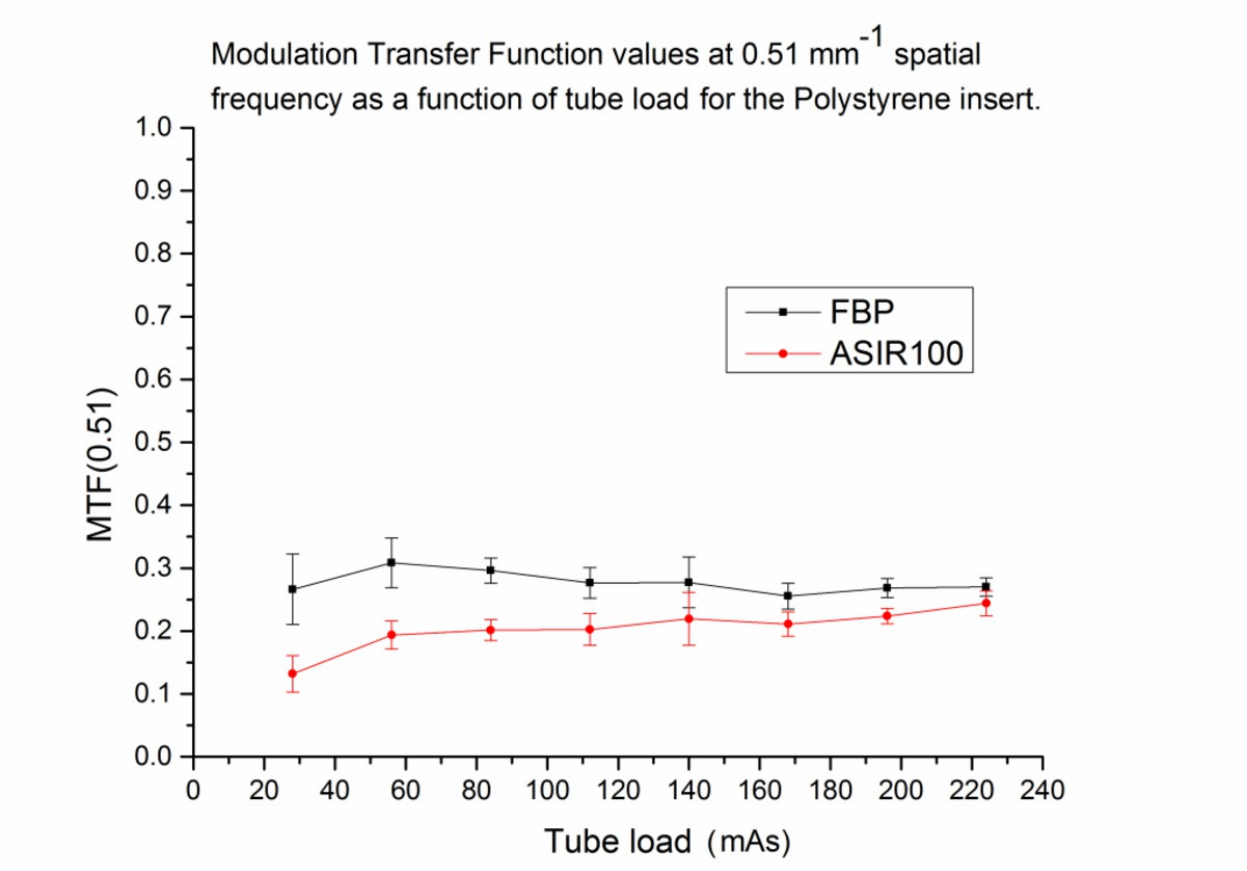

Fig. 29: MTF values at 0.51 mm^-1 spatial frequency as a function of mAs.

Conclusion

In the noise analysis we assessed the performance of ASIR concerning the image noise reduction compared to the standard FBP algorithm. By changing the main scanning parameters (mAs, kV, pitch, slice thickness) we showed that, increasing the ASIR percentage of reconstruction, a greater reduction of the image noise is achieved (up about to 50% with respect to FBP reconstruction) without modifying data trends (i.e. the noise dipendence from these parameters remains the same). Since the dose and the image noise are strictly related in CT imaging, this result can be read in terms of dose reduction with equal or less noise in the images.

The spectral analysis of the noise also shows a shift of the peak of the NPS toward lower frequencies when increasing the ASIR percentage of reconstruction. This behaviour leads to a different noise texture appearance in ASIR-rconstructed images with respect to FBP-reconstructed images, especially for high percentages of ASIR reconstruction.

Both the noise reduction and the shift of the NPS peak at low spatial frequencies should have a positive influence in terms of image quality.

From MTF analysis we evaluated the ASIR performance in terms of spatial resolution compared to FBP reconstruction. The PSF method used for MTF calculations serves as "verification" of the circular edge method, which is seldom used in CT image quality analysis. The agreement between the two methods has allowed us to evaluate the dependency of the MTF from the contrast in a wide range of values.

Our analysis confirmed that the spatial resolution in ASIR reconstructed images is dose- and contrast-dependent, unlike the FBP reconstruction. In fact, the MTF varies as a function of mAs and constrast.

In our analysis we showed that, except in cases of low contrast and low tube load values, the ASIR algorithm does not significantly degrade the spatial resolution with respect to the FBP algorithm.

Finally, we can cocnlude that in most examined situations, when compared to FBP, ASIR allows a relevant noise reduction without appreciably affecting image quality, proposing as a possible means for dose reduction in CT imaging. Although in high-contrast situations ASIR does not considerably degrades spatial resolution (also for low-dose acquisitions), high percentages of ASIR reconstruction are rarely used in practice because of the heavy changes in the image texture [9]. However, for low dose and contrast acquisitions, this alghoritm provides a lower performance compared to FBP in terms of spatial resolution and thus, in these situations, a particular attention in the usage of ASIR reconstruction is required.

Personal information

References

[1] Thorsted M. Buzug, **Computed Tomography, from Photon Statistics to Modern Cone-Beam CT**, Springer, 2008

[2] Jiang Hsieh, **Computed Tomography, Principles, Design, Artifacts and Recent Advances**, SPIE, 2009

[3] Richard S., Husarik D.B., Yadava G., Murphy S.N., Samei E., **Towards task-based assessment of CT performance: system and object MTF across differentreconstruction algorithms**, Med. Phys. 39(7):4115-22, 2012.

[4] Samei E., Richard S., **Assessment of the dose reduction potential of a model-based iterative reconstruction algorithm using a task-based performance metrology**, Med. Phys., 42(1):314-23, 2015.

[5] C. T. Dodge, C. T. Jensen, E. P. Tamm, D. D. Cody, X. Liu, V. Kundra, and X. J. Rong, **How do iterative reconstruction algorithms affect spatial resolution?**, Poster # 17 SCBTMR, 2013.

[6] J. H. Siewerdsen, I. A. Cunningham, D. A. Jaffray, **A framework for noise-power spectrum analysis of multidimensional images**, Med. Phys. 29(11):2655-2671, 2002.

[7] Jiwon Choi, **Measurement of Noise Power Spectra for CT Images Reconstructed with Different Kernels**, Journal of Convergence Information Technology, Vol. 8 Issue 16 p70, 2013.

[8] Saul N. Friedman, George S. K. Fung, Jeffrey H. Siewerdsen, Benjamin M. W. Tsui, **A simple approach to measure computed tomography (CT) modulation transfer function (MTF) and noise-power spectrum (NPS) using the American College of Radiology (ACR) accreditation phantom**, Medical Physics Vol. 40, N. 5, 2013.

[9] Martin J. Willemink, Pim A. de Jong, Tim Leiner, Linda M. de Heer, Rutger A.J. Nievelstein, Ricardo P. J. Budde, Arnold M. R. Schilham, **Iterative reconstruction techniques for computed tomography Part 1: Technical principles**, European Society of Radiology, 23:1623-1631, 2013.

[10] Christophe Argaud, **ASIR: a new reconstruction technique to lower dose without compromize**, ASIR withe paper, GE Healthcare.

[11] Qiao Yang, Nicole Maass, Mengqiu Tian, Matthias Elter, Ingo Schasiepen, Andreas Maier, Joachim Hornegger, **Multi-Material Beam Hardening Correction (MMBHC) in Computed Tomography**, 2013.

[12] Frédéric A. Miéville, François Gudinchet, Francis Brunelle, François O. Bochud, Francis R. Verdun, **Iterative reconstruction methods in two different MDCT scanners: Physical metrics and 4-alternative forced-choice detectability experiments - A phantom approach**, Physica Medica N° 2 p. 99-110, 2013.